Forestry An International Journal of Forest Research

Institute of Chartered Foresters

Forestry 2017; **90**, 613–631, doi:10.1093/forestry/cpx014
Advance Access publication 24 March 2017

Estimating stand density, biomass and tree species from very high resolution stereo-imagery – towards an all-in-one sensor for forestry applications?

Fabian Ewald Fassnacht[1]*, Daniel Mangold[1], Jannika Schäfer[1], Markus Immitzer[2], Teja Kattenborn[1], Barbara Koch[3] and Hooman Latifi[4]

[1]*Institute of Geography and Geoecology, Karlsruhe Institute of Technology, Reinhard-Baumeister-Platz 1, Karlsruhe 76131, Germany*
[2]*Institute of Surveying, Remote Sensing and Land Information (IVFL), University of Natural Resources and Life Sciences, Vienna (BOKU), Peter-Jordan-Strasse 82, Vienna 1190, Austria*
[3]*Remote Sensing and Landscape Information Systems, University of Freiburg, Tennenbacherstrasse 4, Freiburg 79085, Germany*
[4]*Department of Remote Sensing in Cooperation with German Aerospace Center, University of Wuerzburg, Oswald-Kuelpe-Weg 86, Wuerzburg 97074, Germany*

*Corresponding author. Tel: +49-721-608-43828; Fax: +49-721-608-46927; E-mail: fabian.fassnacht@kit.edu

Received 12 December 2016

The estimation of various forest inventory attributes from high spatial resolution airborne remote sensing data has been widely examined and proved to be successful at the experimental level. Nevertheless, the operational use of these data in automated procedures to support forest inventories and forest management is still limited to a small number of cases. The reasons for this are high data costs, limited availability of remote sensing data over large areas and resistance from practitioners. In this review the main aim is to stimulate debate about spaceborne very high resolution stereo-imagery (VHRSI) as an alternative to airborne remote sensing data by presenting: (1) a case study on the retrieval of stand density, aboveground biomass and tree species using a set of easy-to-calculate variables obtained from VHRSI data combined with image processing and nonparametric classification and modelling approaches; and (2) the results of an expert opinion survey on the potential of VHRSI as compared with Light Detection and Ranging (LiDAR), hyperspectral and airborne digital imagery to derive a range of forest inventory attributes. In the case study, stand density was estimated with r^2 = 0.71 and RMSE = 156 trees (rel./norm. RMSE = 24.9 per cent/12.4 per cent), biomass with r^2 = 0.64 and RMSE of 36.7 t/ha (rel./norm. RMSE = 20.0 per cent/12.8 per cent) while tree species classifications with five species reached overall accuracies of 84.2 per cent (kappa = 0.81). These results were comparable to earlier studies in the same test site, obtained with more expensive airborne acquisitions. Expert opinions were more diverse for VHRSI and aerial photographs (Shannon index values of 0.94 and 0.97) than for LiDAR and hyperspectral data (Shannon index values 0.69 and 0.88). In our opinion, this reflects the current state-of-the-art in the application of VHRSI for automatically retrieving forest inventory attributes. The number of studies using these data is still limited, and the full potential of these datasets is not yet completely explored. Compared with LiDAR and hyperspectral data, which both mostly received high scores for forest inventory products matching the sensor systems' strengths, VHRSI and aerial photographs received more homogeneous scores indicating their potential as multi-purpose instruments to collect forest inventory information. In summary, considering the simpler acquisition, reasonable price and the comparably easy data format and handling of VHRSI compared with other sensor types, we recommend further research on the application of these data for supporting operational forest inventories.

Introduction

Over the last two decades, high spatial resolution digital remote sensing data has become more commonly available for natural resources inventories. Spatially highly resolved data from airborne hyperspectral (also called 'imaging spectroscopy') and Light Detection and Ranging (LiDAR) sensors were demonstrated to hold great potential to automatically derive forest information to support tasks related to economical (e.g. by providing structural inventory or forest health related information) and ecological (e.g. habitat or biodiversity mapping) management aspects of forest ecosystems. Typical forest information that can be provided by remote sensing data includes standing timber volume, biomass, stand height, stand density and the detection of dead or stressed trees. Such information is relevant for local forest management decisions but also for national and international

reporting commitments (e.g. concerning carbon balance or within REDD+ activities). While remote sensing is not likely to replace completely field-inventories, it is a valuable tool to complement field surveys with objective and spatially continuous estimates of various forest inventory attributes. However, in order to reach an operational status, remote sensing methods must be accurate, robust and transparent to practitioners; the latter point is little discussed but important because it is they who eventually decide whether or not to integrate remote-sensing information in their management system.

In this context, several sensor systems have been discussed and often widely examined in the remote-sensing community. For example, LiDAR data with its ability to capture structural attributes along with a limited amount of spectral information (via intensity values), has been successfully applied to estimate forest structural attributes. These parameters include for example forest height (Nilsson, 1996; Clark *et al.*, 2004, Falkowski *et al.*, 2006), growing stock volume (Straub and Koch, 2011; McRoberts *et al.*, 2013) and biomass (Dubayah *et al.*, 2010; Hudak *et al.*, 2012; Næsset *et al.*, 2013; Fassnacht *et al.*, 2014). Additionally, LiDAR has demonstrated some potential for estimating vascular plant species richness in forests (Lucas *et al.*, 2010; Lopatin *et al.*, 2016) as well as for classifying and mapping tree species (Ørka *et al.*, 2009; Korpela *et al.*, 2010; Vaughn *et al.*, 2012). The latter has been amongst the core applications of hyperspectral data which allows for capturing subtle differences of spectral vegetation properties with its high spectral resolution. Tree species classification with hyperspectral data has been examined in a large number of case studies in urban (Alonzo *et al.*, 2014) natural (Clark *et al.*, 2005) or managed forests (Fassnacht *et al.*, 2014; Ghosh *et al.*, 2014) and has been reviewed by Fassnacht *et al.* (2016). Further applications of hyperspectral data in forests include the estimation of leaf-chemistry variables (Schlerf *et al.*, 2010; Kalacska *et al.*, 2015), canopy water content (Clevers *et al.*, 2010) as well as the assessment of forest health as affected by insects (Pontius *et al.*, 2008; Fassnacht *et al.*, 2014) or pathogens (Coops *et al.*, 2003). Finally, both LiDAR and hyperspectral data have additionally been applied to delineate single trees in forest stands (Dalponte *et al.*, 2014, 2015) and urban forests (Zhang and Qiu, 2012; Alonzo *et al.*, 2014) which enables not only a subsequent retrieval of single-tree parameters but also an indirect estimation of stand density.

In some studies, merging the high spectral and spatial resolution of hyperspectral and LiDAR data, respectively, could further improve the single sensor results. Examples include Alonzo *et al.* (2014) and Dian *et al.* (2016) for tree species classification and studies reviewed by Man *et al.* (2014) for biomass estimations. However, these improvements were reported in many cases to be limited for both tree species classification (Fassnacht *et al.*, 2016) and biomass estimation (Latifi *et al.*, 2012, 2015). In summary, earlier studies indicated that both structural and spectral information are needed to precisely estimate common forest inventory parameters with some parameters primarily requiring structural and others primarily requiring spectral information. This also matches the practical experiences from field inventories, in which both spectral (or visual, i.e. information retrieved by visual assessment of shape and colour of leaves and woody compartments) and structural (=stem diameter, crown radius, tree height, number of trees/ha) attributes are typically recorded. For most applications, information has to be provided at a comparably high spatial resolution to account for the spatial heterogeneity in forest ecosystems and to match the scale on which practitioners require inventory information. This is one reason for the relative dominance of studies that applied airborne sensors compared with satellite-based approaches in the field of remote sensing-assisted forest inventory research.

However, high quality airborne data are often expensive to obtain. According to Ørka and Hauglin (2016) the price for airborne LiDAR and hyperspectral data currently ranges between ~50–220 €/km² and 100–150 €/km², respectively, though combined acquisitions might be available at lower prices. Airborne multispectral imagery are cheaper at an approximate cost of 30–50 €/km². These digital multispectral imageries are particularly relevant as they continue a long tradition in forestry applications, e.g. manual photo interpretation of aerial photographs and orthophotos was and still is a commonly applied procedure to support operational forest inventories. Albeit less frequent than LiDAR and hyperspectral studies, some recent studies have also presented approaches for an automated analysis of airborne multispectral imagery for extracting forest parameters such as tree species (Waser *et al.*, 2010), growing stock volume (Rahlf *et al.*, 2014; Stepper *et al.*, 2015a, b; Straub and Stepper, 2016), basal area (Stepper *et al.*, 2016) or height changes (Stepper *et al.*, 2015a, b). These studies typically applied stereo image processing and photogrammetric methods. Although they suggested that airborne multispectral imagery is suitable for retrieving some forest attributes, automated approaches to retrieve forest attributes that are mainly related to spectral properties are often hampered by the spectral variability in airborne multispectral data. This variability is mostly caused by varying illumination conditions as well as changing sun-sensor geometry and atmospheric conditions (see Fassnacht *et al.* (2016) and discussed papers herein). These changes occur during the course of a day and are even more pronounced if an airborne survey takes several days or weeks, as it is typically the case in operational scenarios. Similar problems have been observed by the authors of this study for large hyperspectral campaigns which often require extensive pre-processing to create a more-or-less homogeneous dataset. Being an active sensing system, these problems apply less for LiDAR data, which are largely independent of sun-illumination and atmospheric properties. Finally, one common restriction of most of the recent airborne data types is that in many parts of the world they are still not readily available.

In this study, we will review and discuss spaceborne very high resolution (VHR) multispectral stereo-imagery (VHRSI) as a globally available alternative to airborne data for remotely assessing forest inventory attributes at high spatial resolutions. A planned new acquisition of a stereo-dataset of the most recent VHRSI sensor system WorldView-3, which features one of the highest spatial resolutions and largest spatial ranges on the market, currently costs ~50 €/km² (with all 16 spectral bands). This is at the lower end of the costs for a LiDAR acquisition and notably cheaper than the price for a typical hyperspectral dataset. Alternative products from sensors like WorldView-2 (eight spectral bands), Pléiades, IKONOS or Quickbird (all with four spectral bands) are available at even lower prices. As VHRSI data are spaceborne, problems related to varying sun-sensor geometry or atmospheric effects might exist between datasets, but are likely to be irrelevant within a single acquisition. Since the imagery is

recorded in a time-span of several seconds to a few minutes neither weather nor illumination conditions are expected to notably change. This is one of the advantages of VHR data compared with a typical airborne campaign, that entails a notably longer time to cover the same area and thus has to deal with changing conditions and the corresponding effects in the data. Concerning the detail of information on spectral and structural properties of forests, the VHRSI is unlikely to reach the level of a combined hyperspectral and LiDAR dataset. Yet, the optical bands of sensors such as WorldView-2 and WorldView-3 cover some of the key spectral regions in respect to plant traits and the spatial accuracy of photogrammetric products complies with many demands for retrieving structural forest attributes in area-based approaches. This has been demonstrated in earlier studies which showed that VHR and VHRSI can reach similarly high accuracies as LiDAR and hyperspectral data for the retrieval of several forest inventory attributes.

For example, earlier studies demonstrated that the combination of a LiDAR-based digital terrain model (DTM) with a photogrammetric digital surface model (DSM) obtained from VHRSI enables good estimations of forest height (RMSE = 1.5–4 m) in many forest ecosystems including Mediterranean pine plantations (Beguet *et al.* 2014), boreal forests (Persson and Perko, 2016) and mangrove forests (Lagomasino *et al.*, 2016). At stand level, good results have also been reported for estimating timber volume (normalized RMSE (nRMSE) = 19.5–27.9 per cent) (Straub *et al.*, 2013; Immitzer *et al.*, 2016; Persson, 2016) and aboveground forest biomass (nRMSE = 11.9–18.3 per cent) (Kattenborn *et al.*, 2015; Maack *et al.*, 2015) with area-based approaches in temperate and boreal forests.

Several studies reported forest density estimations from VHR data with mixed success. For example, Ozdemir and Karnieli (2011) reached only moderate accuracies (r^2 = 0.38, RMSE (nRMSE) = 110 trees (20.9 per cent)) for estimating the number of trees in Aleppo pine (*Pinus halepensis* Mill.) plantations using mainly texture measures from WorldView-2 data. Contrasting results were shown in Beguet *et al.* (2014) who reported high accuracies (r^2 of 0.96 and 0.79 and RMSE (nRMSE) values of 0.37 m (7.7 per cent) and 0.89 m (18.6 per cent) for two examined sites in southern France) for estimating tree spacing in Mediterranean pine plantations using textural and spectral features from Pléiades and Quickbird data.

Finally, VHR data have also been applied to classify and map tree species. Recent studies include the works of Cho *et al.* (2015) who classified three dominant tree species and three other relevant classes (bushes, bare soil and burnt patches) in an indigenous forest in South Africa. They applied WorldView-2 data and reported high overall accuracies (OA) of 89.3 per cent. Peerbhay *et al.* (2014) also reported high overall classification accuracies of 85.4 per cent (kappa = 0.8) for classifying six tree species (including four eucalyptus and two pine species) from WorldView-2 data for a test site near to the one examined in Cho *et al.* (2015). Similarly, high accuracies were reported by Immitzer *et al.* (2012) for 10 tree species or Waser *et al.* (2014) for seven species both in temperate central European forests. They reached on average higher accuracies for coniferous than for broadleaved trees. Immitzer *et al.* (2012) as well as Pu and Landry (2012) emphasized the importance of the four additional WorldView-2 bands in the blue, yellow and near infrared portions of the spectrum for classifying tree species.

In addition to the above examples, VHR data has been suggested as a tool to support forest health monitoring (Waser *et al.*, 2014; Immitzer and Atzberger, 2014), LAI estimation (Zhou *et al.*, 2014; Pu and Cheng, 2015) or the mapping of areas being felled (Chirici *et al.*, 2011).

In summary, the potential of VHR and VHRSI data to retrieve a range of important forest inventory attributes has been presented in earlier studies. Nevertheless, the possibility of applying these data in operational surveys has been discussed far less than the application of airborne LiDAR and hyperspectral data (see, e.g. Holopainen *et al.*, 2014 and Lim *et al.*, 2003). This was the motivation for this study, which aims to inform and stimulate the debate about the potential of VHR and VHRSI by combining the findings of a case study with a more general discussion on the current opinions concerning the operational use of VHRSI data for forest inventory tasks.

The study has three aims:

(1) Present straightforward approaches to estimate forest inventory parameters (stand density, aboveground biomass, tree species) from stereo WorldView-2 imagery using a combination of field data, image processing, photogrammetry and machine learning methods;
(2) discuss the methods and findings of our local case study with earlier results obtained from airborne LiDAR and hyperspectral data also considering a more applied practitioner's perspective; and
(3) position the local findings in a wider context based on an expert opinion survey on the suitability of the four commonly available sensor systems (LiDAR, hyperspectral, VHRSI and digital aerial imagery) for forest inventory tasks.

Study area

The study area is located in the Hardtwald forest in the north of the city Karlsruhe, southwestern Germany (49° 0′ 34″ N, 8° 24′ 14″ E) (Figure 1). The site has a temperate climate with an average annual temperature of 10°C and an annual precipitation of 800 mm. The study site has been described in several earlier studies (Heinzel and Koch, 2011; Fassnacht *et al.*, 2014). The area is located in flat terrain and forests are stocked with pure and mixed stands of predominantly Scots pine (*Pinus sylvestris* L.), European beech (*Fagus sylvatica* L.), oaks (*Quercus petraea* (Matt) Liebl., *Quercus robur* L.), red oak (*Quercus rubra* L.) and hornbeam (*Carpinus betulus* L.) with a small component of Douglas-fir (*Pseudotsuga menziesii* (Mirb.) Franco), European larch (*Larix decidua* Mill.) and silver birch (*Betula pendula* Roth). The age of the stands is varied and ranges between 30 and 150 years. Based on earlier surveys, two and three-layered stands are common amongst the older parts of the forest exceeding 100 years.

Materials

Remote sensing datasets

The applied remote sensing datasets included two WorldView-2 scenes featuring eight multispectral (pixel size of 2 m) and one panchromatic band (pixel size of 0.5 m) as well as a LiDAR DTM with a pixel size of 1 m.

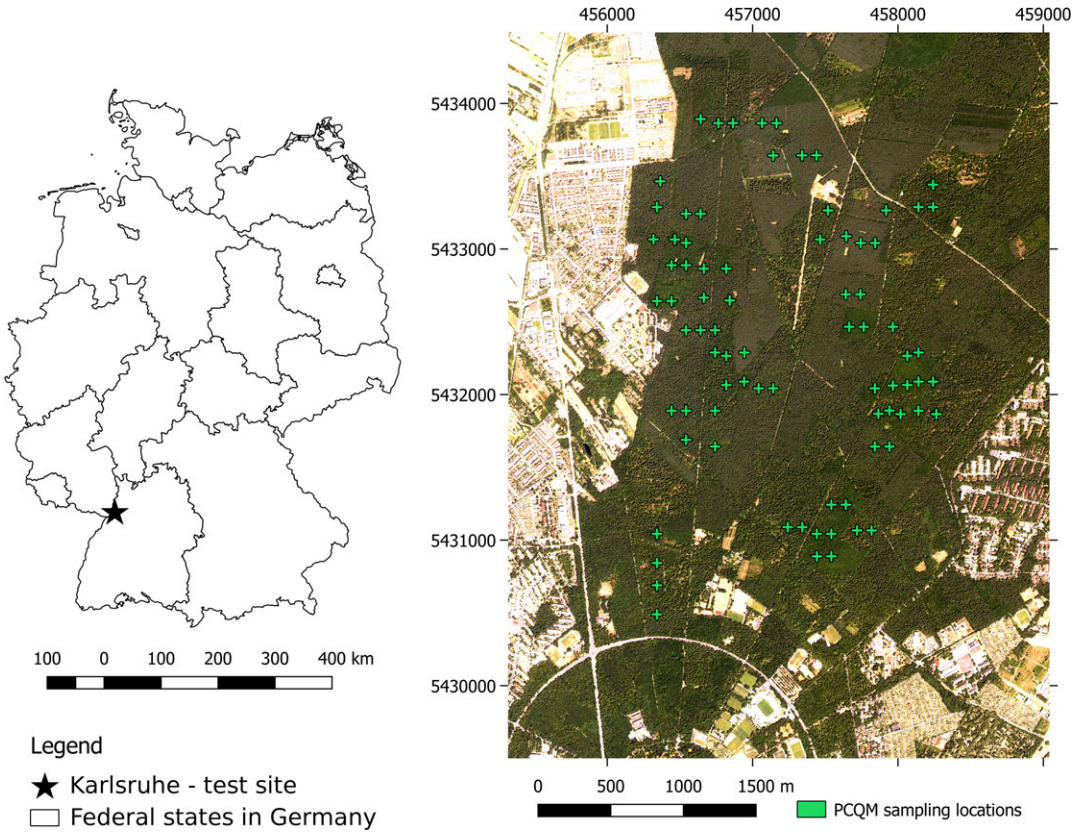

Figure 1 Location of the test site in Germany (left) and WorldView-2 RGB composite view of the test site (right).

The eight multispectral bands of the WorldView-2 scenes cover a spectral range between 400 and 1040 nm, while the panchromatic band measures total radiation between 450 and 800 nm. The two scenes were acquired on the 8th and 23rd of June 2013. The earlier scene contained ~10 per cent cloud-cover. The DTM originated from LiDAR point-cloud data collected over the study area with a Riegl LMS-Q560 laser scanner mounted on a Harrier 56 system (see Latifi *et al.*, 2012 for further details).

The two WorldView-2 scenes were used as a (repeat-pass) stereo-pair to obtain a photogrammetric DSM. We applied the ERDAS LPS module (Leica Geosystems, Atlanta, Georgia, USA) to derive a photogrammetric point cloud from the two panchromatic bands of the WorldView-2 data. The point cloud was then interpolated using TreesVis (Weinacker *et al.*, 2004). This resulted in a DSM with a pixel size of 1 m. To obtain a normalized DSM (nDSM), the LiDAR terrain model was subtracted from the WorldView-2 DSM. Prior to this, we accounted for a small height off-set between the two datasets by first quantifying the offset within areas covered by asphalt and bare ground and then subtracting the offset from the LiDAR DTM.

Reference field data

Two field surveys were conducted in the study area in 2015 to obtain reference data for aboveground biomass, stand density and tree species. The two campaigns have a 2-year offset between field data and satellite acquisition. However, considering the relatively stable conditions in the study site (there were no major storm events or harvests in the last few years), the effects caused by this time lag were assumed to be very small and were not taken into account.

Tree species

Tree species reference data were collected at the single-tree level. The single trees were first delineated from the cloud-free pan-sharpened WorldView-2 image. Existing forest inventory maps of the study area were used to stratify the delineated crowns based on tree species. Furthermore, it was ensured that the delineated crowns are well spread over the whole study area. We tried to mainly delineate crowns that we assumed to be relatively easy to identify in the field. This in turn introduces a bias to the finally selected crowns, as there was a tendency towards larger tree crowns overtopping the surrounding canopy. However, we also delineated co-dominant crowns in mono-species stands in which the identification of the individual trees in the field was considered to be unnecessary. It was assumed that a verification was sufficient at the rough location of the delineated crowns to ensure that no other species occurs in the area. A field survey was conducted in April 2015 to confirm the species of each delineated crown. Furthermore, the location and species of additional trees were recorded during the survey. An accurate delineation of these trees was accomplished afterwards. The survey resulted in a total of 348 reference trees of 10 species (Table 1).

In addition, 33 and 13 sample pixels were directly collected from the cloud-free WorldView-2 image for shaded and bare

Table 1 Summary of tree species reference data.

Tree species	Number of reference crowns
Red Oak (*Quercus rubra*)	59
European Larch (*Larix decidua*)	55
Oak (*Quercus robur*, *Quercus petraea*)	53
Scots Pine (*Pinus sylvestris*)	43
Hornbeam (*Carpinus betulus*)	31
European Beech (*Fagus sylvatica*)	29
Douglas Fir (*Pseudotsuga menziesii*)	28
Norway Maple (*Acer platanoides*)	21
Silver Birch (*Betula pendula*)	17
Linden (*Tilia grandifolia, Tilia cordata*)	12
Shadow	33 (point samples)
Bare ground	13 (point samples)

ground areas, respectively. These classes were added to account for the commonly occurring shadowed and bare ground patches in the forest that would otherwise be misclassified as one of the species in the applied supervised classification. The shadow samples were collected within all common forest types, while a low number of samples were considered to be sufficient for an accurate description of the bare ground signal.

Stand density

To obtain reference data for stand density, a field survey was conducted using the Point-Centred Quarter Method (PCQM) described in Mitchell (2001). The PCQM is a plot-less method based on repeated measurements along transects. The approach is simple and fast, and has been reported to have statistical advantages over comparable methods (Beasom and Haucke, 1975; Mitchell, 2001).

The PCQM was conducted as follows:

(1) A list with random numbers between 1 and 100 was created and sorted in ascending order.
(2) A transect with a length of 100 m was established in a given forest stand using a tape measure.
(3) The surveyors started at the beginning of the transect (tape measure) and walked until they reached the first random number in metres.
(4) At this first measurement point an imaginary orthogonal line was set on the transect resulting in four sectors (Figure 2).
(5) In each of the four sectors, the closest tree to the measurement point with a diameter at breast height (DBH) of greater than 7 cm was recorded by noting its species, DBH and distance to the measurement point.
(6) The surveyors walked to the next random number and repeated steps (4) and (5). Measurement points always had to be at least 4 m apart from each other. Random numbers that fell in-between were dropped.

Here, the PCQM method was applied to record reference data at 80 locations within the study area in summer 2015. The locations were selected based on an earlier experimental design (Kattenborn *et al.*, 2015). Available inventory information for these locations served as orientation to ensure that all major

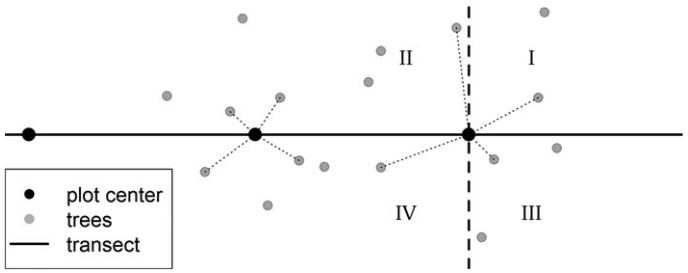

Figure 2 Scheme of the PCQM method (following Mitchell 2001).

forest types of the study site were sampled. This explains the irregular distributions of the sampling locations (Figure 1). Plot locations were recorded with a standard GPS (Garmin Maps 64S). At each location two transects were sampled: one in a north-south direction and one in an east-west direction. Based on the recorded data we calculated the overall stand densities (trees/ha) following the equations given in Mitchell (2001). For the calculation of stand density, the two transects per plot were treated as a single dataset.

Biomass

Reference data for aboveground biomass (t/ha) were obtained from the same PCQM data used to record the reference for tree density. Biomass estimates were derived by first calculating biomass values for each recorded tree using species-specific allometric equations. The equations required only the DBH of the measured trees as input parameters (Jenkins *et al.*, 2003; Zianis *et al.*, 2005; Zell, 2008; Annighöfer *et al.*, 2012). Then the biomass of an average tree was calculated for each species occurring in a PCQM sample. These values were then extrapolated to tons per hectare values by multiplying the median tree biomass with the species-specific tree densities of each PCQM sample as obtained from the PCQM method. Trees that were measured several times during the PCQM were considered only once to derive the median tree biomass. Furthermore, from the 5140 measured trees we excluded 52 trees below and above the 1st and 99th percentiles of biomass values, respectively. Preliminary experiments showed that such outliers (especially very large individuals) have a notable effect on the estimated tons per hectare biomass values which hampers a combination of the reference data with the remote sensing predictors. For example, in one sample, a single oak tree with a DBH of almost 1 m had an estimated biomass of almost 9 t, while all other trees did not exceed 2.3 t with the majority of the trees showing biomass estimates of less than 500 kg. In such cases, an individual tree can have a notable effect on the extrapolated biomass estimates per ha which can lead to values that do not represent the situation in the stand.

Sample-based biomass estimates generally suffer from these problems and further uncertainty is added by the allometric equations, which also build on empirical relationships that can notably vary with location. Hence, the biomass reference dataset is likely to contain an unknown degree of uncertainty. This uncertainty could be reduced by developing site-specific biomass equations through destructive sampling and by replacing the sample-based survey with a full survey during which each

tree of a sample plot is measured. However, both suggestions would lead to a notably increased workload that could not be matched with the resources available in this study. A statistical summary of the two reference sets obtained during the PCQM survey is given in Table 2.

Methods

The WorldView-2 scenes were processed in three processing chains to derive three forest inventory parameters as summarized in Figure 3 and discussed in detail below.

Table 2 Statistical summary of biomass and tree density values of the PCQM survey.

	Min.	Max.	Mean	Median
Biomass (t/ha)	33.5	346.4	180.1	190.9
Biomass (t/ha) (two outliers removed)	50.1	336.4	183.9	198.1
Stand density (Trees/ha)	143	1397	626	586

Tree species classification

For the tree species classification, we applied a work-flow described in detail in earlier studies (Fassnacht *et al.*, 2014, 2015). In summary, we applied a support vector machines (SVM) classification with a radial basis function (RBF) kernel. The SVM was optimized for sigma and cost via a grid search. Classification accuracies were obtained via a fivefold cross-validation and an additional iterative procedure based on bootstrap resamples of 100 splits of the reference data into training and validation datasets. The latter approach helps to capture the variability in classification accuracy as a function of the composition of training and validation sets. This variability has been shown to be quite high in the case of limited sample sizes (Fassnacht *et al.*, 2016). The pixel-wise classification maps were obtained from a separate classification that applied all reference data in the training stage to exploit all available information.

The input variables to the SVM classification included the eight WorldView-2 spectral bands as well as eleven textural metrics obtained from the panchromatic channel via the standard grey-level co-occurrence matrix procedure available in ENVI 4.8 (ITT Visual Information Solutions, 2009). We applied a window size of 9 (= 5.5 m) which conforms roughly the average crown diameter in the study area. The eleven texture measures were subsequently resampled to a pixel size of 2 m and were stacked with the spectral bands.

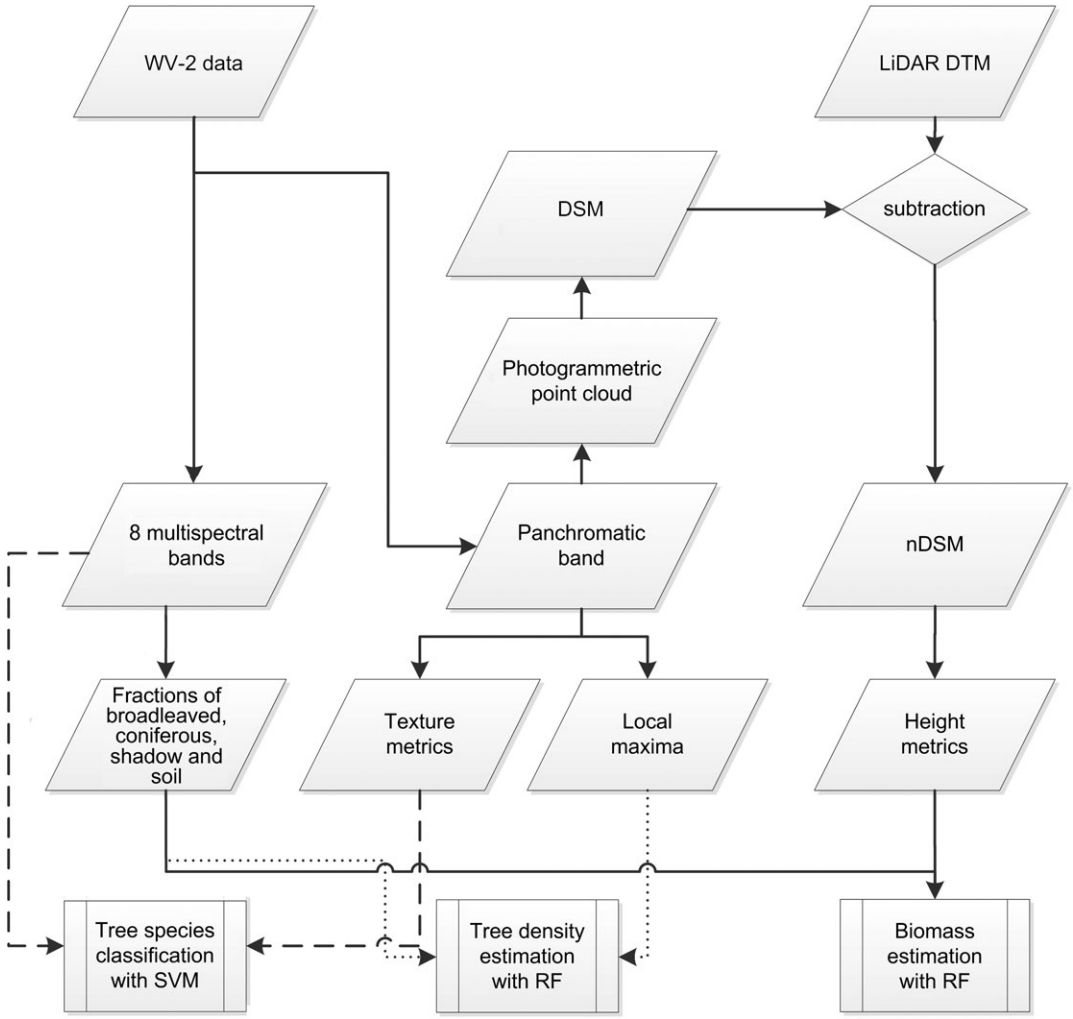

Figure 3 Overview of the methodical work-flow.

The reference crown-polygons and the additional sample points for shadow and bare ground pixels were overlapped with the image stack consisting of spectral and textural bands, and mean values of each band were extracted for all pixels intersecting with the crown polygons. These data served as input to the subsequent classification. Classification maps were obtained by applying the trained SVM algorithm pixel-wise to the WorldView-2 image stack containing the spectral and textural bands.

In total three classifications were tested. Classification A applied reference crowns from all available species; Classification B used only five mostly stand dominating species that had also been examined in earlier studies using hyperspectral data (Ghosh *et al.*, 2014; Fassnacht *et al.*, 2014); and Classification C considered two broad groups of broadleaved and coniferous trees (see Methods for stand density). In all scenarios bare ground and shadow were considered as additional classes, as previously described.

Stand density estimation

To estimate the number of trees per ha, we derived two types of variables from the WorldView-2 imagery. Both variables were extracted at the areas where the PCQM was conducted. The PCQM areas were defined with a buffer around the two perpendicular transects. The radius of the buffer was first defined as 7.85 m (the 90th percentile of all tree distances measured during the PCQM) but an additional 3 m was added later resulting in a radius of 10.85 m. The additional 3 m increment was added to account for GPS inaccuracies which are commonly observed in forests (Tomaštík *et al.*, 2016).

The first examined variable type was the number of local maxima obtained from filters with a window size of 7 by 7, 9 by 9 and 11 by 11 pixels that were applied to the panchromatic bands of the cloud-free WorldView-2 scene (the predictor obtained with a window size of 9 by 9 pixels was used in the final model) (Figure 4a). The window sizes were selected to approximately match the average size of a single tree crown. Each maximum was assumed to represent a tree top that leads to a local maximum reflectance due to its exposed position. Similar approaches had been presented in earlier studies (Patias and Stournara, 2016).

The second examined variable type was obtained from a simple classification with the four classes of broadleaved trees, coniferous trees, shadow and soil (Figure 4b). Here, we followed the procedure described for the tree species classification but used an independent reference dataset containing 35, 37, 32 and 39 samples for the classes broadleaved, coniferous, shadow and bare ground, respectively. These reference samples were directly generated by visual interpretation using a false-colour-composite view of the cloud-free WorldView-2 scene. We are confident that these simple classes could be reliably collected via image interpretation and additionally considering available forest inventory maps. The corresponding classification accuracies are reported in the Results section (classification C of the tree species classifications). From the obtained classification map, we calculated the fractions of each of the four classes within each PCQM area. We assumed that the fractions of shadow and bare ground might be associated with the density of the stand and hence would be suitable predictors to estimate the number of trees per ha. Furthermore, we assumed that the information on forest types could also be relevant in the biomass models (see below).

We applied the Random Forest (RF) regression algorithm for modelling, which is a well-known machine learning method for which detailed information can be found in earlier literature (Breiman, 2001; Hastie *et al.*, 2009). The algorithm was parametrized with number of variables randomly sampled at each split (mtry) = 2 and number of trees per forest (ntree) = 500. The explained variances based on out of bag model validation are reported along with Pearson's r^2 and RMSE values calculated between RF predictions and reference values. Since our sample size was limited, we did not conduct a fully independent validation but relied on the bootstrap-based out-of-bag validation as an adequate validation method which has been used in earlier publications (Breiman, 2001; Immitzer *et al.*, 2016).

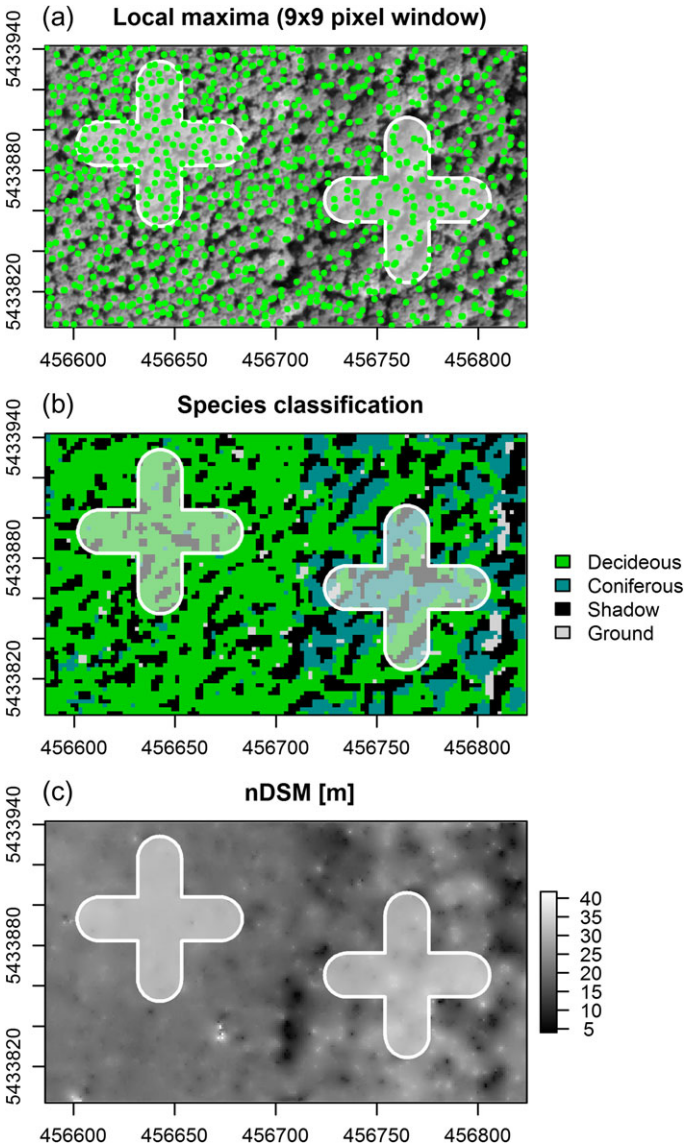

Figure 4 The three predictor variable types applied for model building: (a) the number of local maxima obtained from the panchromatic band of the WorldView-2 imagery; (b) fractions of deciduous, coniferous, shadow and bare ground pixels; and (c) height variables extracted from the photogrammetric nDSM.

To check for the robustness of this approach, we additionally repeated the whole procedure for the clouded WorldView-2 imagery but excluded the PCQM areas that were affected by clouds. To obtain fractions of broadleaved, coniferous, shadow and bare ground, we applied the same number of samples collected from approximately the same locations as for the cloud-free WorldView-2 imagery. However, the locations had to be slightly adapted, as for example shadows did not occur at exactly the same locations in the two images. Moreover, a few points that would have been affected by clouds were also shifted. The best model for the clouded scene was found by combining the fractions of

broadleaved, coniferous, shadow and bare ground with the 'Local Maxima' variable obtained with the 11 by 11 pixels window.

Biomass estimation

RF was also applied to model forest biomass, with identical parameters to those that were used to estimate stand density. The predictor variables included mean, median, and standard deviation of height values of all pixels within the PCQM areas as extracted from the WorldView-2-derived nDSM (Figure 4c). In addition, the fractions of broadleaved, coniferous, shadow and bare ground as well as the number of local maxima as described in the stand density model were used as predictors. The model validation also followed that of the stand density models.

Before estimating biomass, we excluded 12 of the 80 field PCQM samples, since 10 of them were affected by cloud-cover (and hence no reliable height could be extracted for these areas) and two points were excluded as outliers after preliminary examination (results including the outliers are presented in Supplementary material 5).

Prediction maps were obtained by first creating a regular grid of polygons with the area of a single grid cell matching the area of a PCQM sample. Then all predictor variables were derived for these grid cells and the RF models for biomass and stand density were applied to the grid.

Expert opinion survey

To put the results of the case study into a wider perspective and to understand how the remote sensing community perceives the potential of VHRSI data for forestry applications, we invited 35 international remote sensing experts working at the interface between forestry and remote sensing to participate in an expert opinion survey. The invited experts were a mix of senior scientists with outstanding reputation in the field of forest remote sensing and a number of additional experts who recently published VHRSI related works in peer-reviewed international journals. Of the 35 contacted experts 22 replied to our emails. The participants were asked to fill a table in which the potential of four sensor types (airborne LiDAR, airborne hyperspectral, VHRSI and airborne digital imagery) to estimate a range of forest parameters (Supplementary Data 1) should be rated on an ordinal scale with four classes (Table 3). The experts were asked to complete the table, assuming (semi-) automated methods and an operational use of the corresponding remote-sensing sensor types to estimate the defined forest parameters.

Furthermore, the experts were asked to focus their feedback to one of the three most commonly occurring global forest biomes (boreal, temperate and tropical forests). From the 22 replies we received, four experts were commenting on tropical forests while for boreal and temperate forests we received 5 and 13 replies. The results of the survey are reported in histograms, showing the frequency of the four classes for each sensor type and forest parameter. In addition, we report mean values for each sensor type, forest parameter and biome. Finally, we calculated the Shannon Index of Entropy to quantify the diversity in the opinions of the experts. The Shannon Index is defined as follows:

$$H_S = \sum_{i=1}^{s} p_i * \ln(p_i)$$

where in the given case, s is the total number of ordinal classes and p_i is the proportion of votes belonging to the i^{th} ordinal class. The higher the index the more diverse are the expert opinions on a given combination of sensor type and forest parameter.

Table 3 Ordinal classes of the expert opinion survey.

Class	Ordinal class	Definition
1	Poor	Hardly any potential, might work in a few exceptional situations
2	Limited	Works but does not reach the accuracy demanded by practitioners, yet could serve as a supplementary information (e.g. for separating broad forest type classes instead of species)
3	Good	Works good and over many forest types, reaches accuracy demands in most cases, might not work in a few exceptional situations
4	Excellent	Works very good and over all forest types, matches accuracy demands, with marginal problems in very few cases

Results

Tree species classification

Table 4 summarizes the performances of Classifications A to C. In general, better mean classification accuracies were observed for the fivefold CV, compared with those obtained by the iterative bootstrap resampling. However, all results achieved by the fivefold CV were in the range of observed bootstrap results.

Classification A, involving 10 species, reached moderate OA of greater than 70 per cent, whereas the reduction to five tree species (Classification B) reached results of greater than 80 per cent. The broadleaved and coniferous species groups were even classified with perfect accuracies, reaching 100 per cent for the fivefold cross-validation.

Table 4 Summary of tree species classification results.

Classification accuracy measure	A (10 species)	B (five species)	C (broadleaved/coniferous)[1]
Overall acc. (fivefold CV)	79.7%	85.7%	100% (100%)
Mean overall acc. (iterative bootstrap)	73.8%	84.2%	99.8% (98.4%)
St. dev. (iterative bootstrap)	8.1%	3.8%	0.6% (1.7%)
Mean kappa (iterative bootstrap)	0.71	0.81	0.99 (0.98)
St. dev. kappa (iterative bootstrap)	0.08	0.05	0.01 (0.02)
Min./max. user's acc.	0.0%/100%	25.0%/100%	85.7%/100% (81.8%/100%)
Min./max. producer's acc.	0.0%/100%	18.2%/75.8%	87.5%/100% (81.8%/100%)

[1]Results of clouded scene are given in brackets.

Moreover, the distributions of user's accuracy (UA) and producer's accuracy (PA) values obtained in the bootstrap validation showed low classification accuracies for some classes in Classification A (Supplementary Data 2). In particular, Linden and Hornbeam reached only low mean accuracies of less than 50 per cent.

In Classification B, involving five dominant species, all species reached mean UA and PA values of over 60 per cent in the bootstrap validation, with most species showing mean UA and PA values of higher or close to 80 per cent (Figure 5).

The classification map from Classification A showed a rather heterogeneous pattern with frequent misclassifications that even occurred in homogeneous stands (results not shown here). For Classification B (Figure 7 and Supplementary Data 3), the maps generally agreed well with known species occurrences within pure stands. In mixed stands however, a certain over-estimation of Oak was observed, as field observations revealed that most mixed old-growth stands are stocked with Beech rather than with Oak. These misclassifications are also reflected in the confusion matrix (Table 5) where highest confusion occurs between the three broadleaved species (Oak, Beech and Red Oak).

Stand density estimation

The model to estimate stand density reached good accuracies of r^2 = 0.71 (Pearson's r^2 between observed and predicted values) and RMSE = 156 trees/ha. Figure 6 indicates only a slight model bias to underestimate high stand densities.

These model results were robust across the two examined scenes, since the model for the cloud-affected WorldView-2 scene reached comparable results to that of the cloud-free scene (r^2 = 0.69, RMSE = 146 trees/ha). The good model fits were also reflected in the final prediction map (Figure 7). In the displayed subset of the stand density map (Figure 7d), high densities of trees are predicted for comparably young and dense stands in which individual crowns are hardly identifiable in the panchromatic view (Figure 7a). In contrast, notably lower number of trees per ha were predicted in areas where large individual crowns were clearly visible in the panchromatic view.

The predictors that notably contributed to the results were the 'Fraction of Shadow' and 'Fraction of Bare Ground', both showing negative correlations with tree density and the 'Local Maxima with a Window Size of 9' showing positive correlations with stand density (Table 6).

Biomass estimation

The biomass estimations reached reasonable accuracies of r^2 = 0.64 (Pearson's r^2 between observed and predicted values) and RMSE = 36 t/ha (Figure 8). Similar to the stand density model, the biomass model showed a slight bias indicating that the model has slightly overestimated small biomass and underestimated high biomass values.

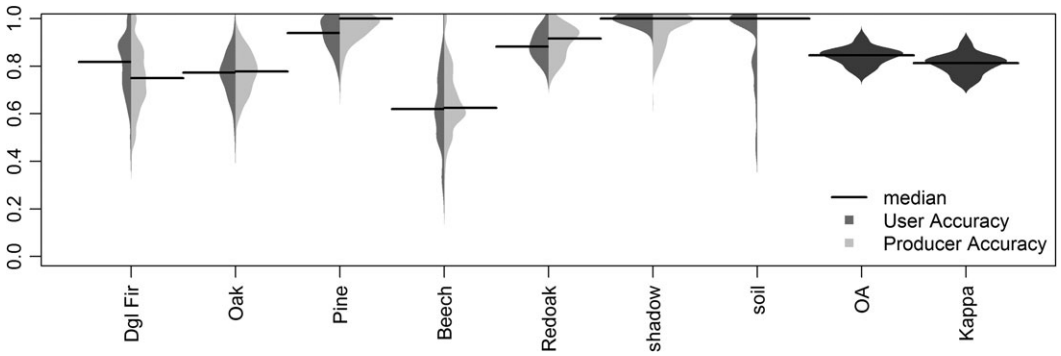

Figure 5 Distributions of user's accuracy and producer's accuracy values for all considered classes as well as overall accuracy (OA) and kappa for Classification B.

Table 5 Aggregated confusion matrix for Classification B as obtained from the 100 classifications.

Class. \ Ref.	Dgl. Fir	Oak	Pine	Beech	RedOak	Shadow	Soil	User. Acc.
Dgl. Fir	**834**	98	67	136	1	0	0	*73.4%*
Oak	53	**1482**	37	187	182	0	4	*76.2%*
Pine	43	28	**1464**	1	0	1	0	*95.3%*
Beech	111	184	0	**639**	70	2	0	*63.5%*
RedOak	0	144	0	80	**1966**	0	0	*89.8%*
Shadow	0	11	0	0	3	**1185**	57	*94.3%*
Soil	0	0	0	0	0	0	**412**	*100.0%*
Prod. Acc.	*80.1%*	*76.1%*	*93.3%*	*61.2%*	*88.5%*	*99.7%*	*87.1%*	***OA**: 84.2%*

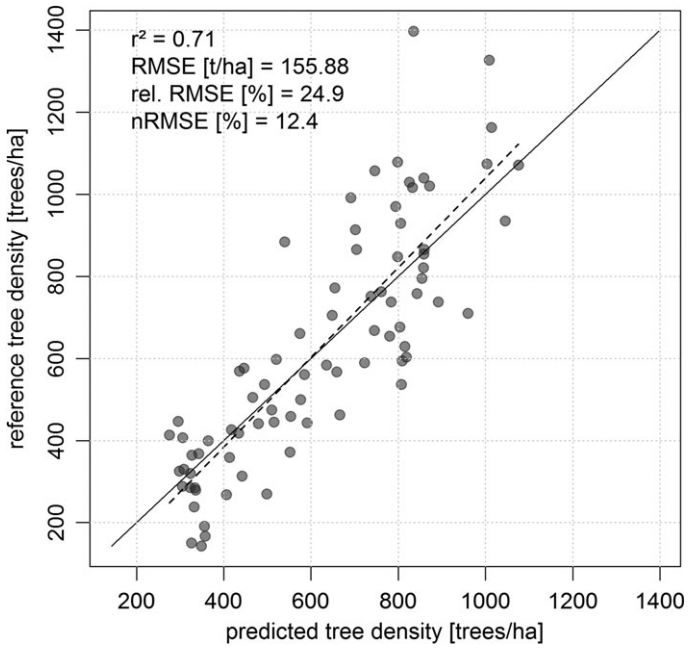

Figure 6 Scatterplot between predicted and observed stand density. Solid line indicates the one-to-one line; dashed line indicates the linear model between values predicted by the Random Forest model and reference values.

The predicted biomass patterns (Figure 7b) generally agreed with field knowledge and earlier LiDAR-based studies conducted in the study area (Fassnacht *et al.*, 2014). The highest biomass values were observed for intermediate density, mixed and high old-growth stands. Predictors with highest correlations to biomass included 'Fraction of Shadow', 'Fraction of Broadleaved Trees', 'Fraction of Coniferous Trees' and 'Median and Mean Height' with only 'Fraction of Broadleaved Trees' showing a negative correlation with biomass (Table 7).

Expert opinion survey

Experts assigned the overall highest average scores (considering all forest variables and all biomes) to LiDAR data (average of 2.8), followed by aerial photographs (2.3), VHRSI (2.2) and hyperspectral data (2.0). Concerning the individual forest attributes, experts judged that LiDAR data has the highest overall potential for the estimation of 'Stand Height' followed by 'Canopy Cover' and 'Wood Volume'. LiDAR received low scores (1.0–1.7) for 'Leaf chemistry', 'Forest Health' and 'Species'. Hyperspectral data received high scores for retrieving information on forest health (3.1), species (3.0) and leaf chemistry (3.1), whereas the potential for all other parameters was only limited or poor (1.2–2.4). VHRSI and digital aerial images both received comparable scoring patterns with intermediate potential (2.2–3.2) for many forest parameters and with only three variables ('Leaf Chemistry', 'Multi-layer Detection' and 'Understorey Detection') scoring below 2.0 (Table 8).

The scoring fluctuations between biomes were low with the majority of the cases showing scoring differences of less than 0.5 (22 cases) or between 0.6 and 0.9 (15 cases). Exceptions include hyperspectral potential for assessing leaf chemistry which received high scores for tropical forests (3.5) and lower scores for boreal forests (2.5) as well as VHRSI's and Aerial Photographs' potential for 'Forest Height' which received high scores for temperate forests (2.9 and 3.4) and low for tropical forests (1.8 and 2.2).

The diversity of the expert opinion's varied with sensor type and forest parameter. Considering all parameters, LiDAR showed clearly lowest diversity (0.69) followed by hyperspectral (0.88), VHRSI (0.94) and aerial photographs (0.97). These patterns are also reflected in the histograms displayed in Figure 9. Highest diversities were observed for 'Canopy Cover' from hyperspectral data, 'Stand Density' from aerial photographs and VHRSI, 'Wood Volume' from aerial photographs and VHRSI as well as 'Stand Height' from VHRSI and 'Leaf Chemistry' from hyperspectral data (Table 9).

Discussion

In this study, we reported satisfactory results for estimating three essential forest inventory parameters, including stand density (trees/ha), aboveground forest biomass (t/ha) and tree species by means of VHRSI. The main discussion point to arise from this is the potential ability to operationalize this approach and compare it to the published results from airborne remote sensing systems.

Tree species classification

The tree species classification including spectral and textural information revealed good results. The obtained accuracies for the classification of 10 tree species are in line with similar studies in Central Europe. The OA of nearly 80 per cent is only slightly lower than those achieved by Waser *et al.* (2014) for seven tree species (OA = 83 per cent) or by Immitzer *et al.* (2012) for 10 tree species (OA = 82 per cent). Only studies with a small number of tree species reached higher values such as Cho *et al.* (2015) for three species or Peerbhay *et al.* (2014) for six tree species (OA = 89 and 85 per cent, respectively). Also in this study a reduction to the five main tree species caused an increase of the obtained OA to ~85 per cent, which is similar to earlier studies in the same test site using hyperspectral data. Ghosh *et al.*, 2014 and Fassnacht *et al.*, 2014 obtained OAs of 86 and 96 per cent, respectively for the same tree species in the same forest.

The analyzed tree species showed large differences in the class specific accuracy values. In the model analyzing 10 species Scots pine, European larch, Douglas-fir and silver birch revealed very good results, Norway maple (*Acer platanoides* L.) and oak acceptable accuracies. The lowest UA and PA were found for linden (*Tilia cordata* Mill., *Tilia grandifolia* Ehrh. ex W.D.J. Koch), hornbeam and European beech. Immitzer *et al.* (2012) achieved also only low accuracy values for hornbeam but very good results for European beech, which was the dominant tree species at their test site (linden was not analyzed). We observed a general tendency that class specific accuracies (UA and PA) increased for species with more samples. Hence, to harness the high potential of VHR data for tree species classification an adequate number of reference samples with high quality is indispensable.

Further improvements of the classification models could be obtained by integrating texture measures that are explicitly designed to differentiate between certain tree species. Such measures have been proposed for airborne digital imagery (Zhang and

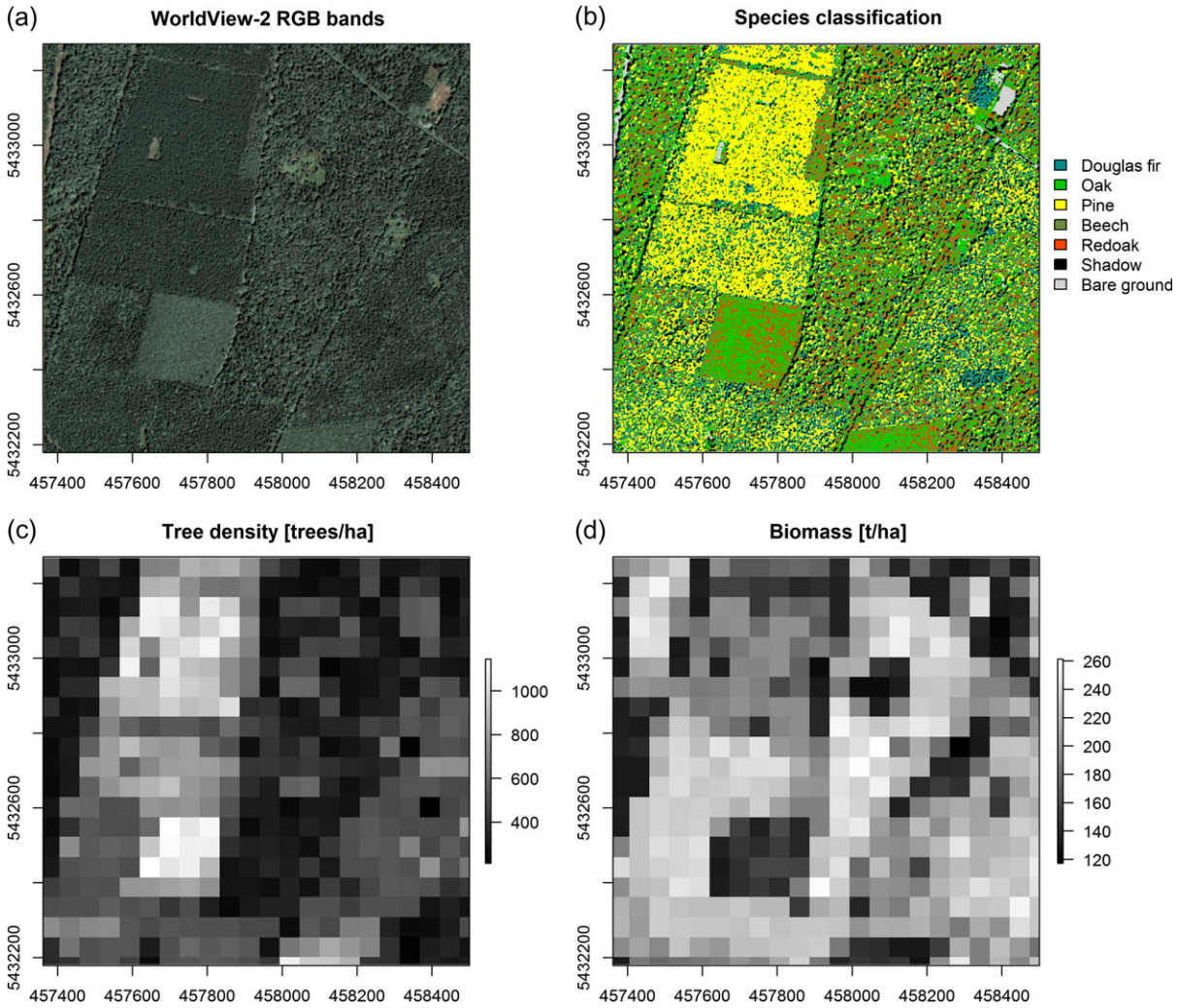

Figure 7 Overview of all results obtained from the stereo WorldView-2 data for a subset of the study area including a RGB-composite of the pan-sharpened WorldView-2 data as reference (a), the tree species classification map (b), the tree density map (c) and a map depicting the biomass distribution (d).

Table 6 Spearman rank correlation coefficient between predictor variables and field-estimated tree density. Predictors not used in the final model are shown in grey.

Predictor	Spearman rank correlation with tree density – cloud-free WorldView-2 scene	Spearman rank correlation with tree density – cloud-affected WorldView-2 scene
Fraction of broadleaved trees	–0.03	–0.12
Fraction of coniferous trees	0.11	0.17
Fraction of shadow	–0.70	–0.61
Fraction of soil	–0.56	–0.75
Local maxima (window size = 7)	0.67	0.74
Local maxima (window size = 9)	0.80	0.80
Local maxima (window size = 11)	0.76	0.80

Hu, 2012) and could be adapted to VHR data. However, the current limitation to 0.3 m pixel size (WorldView-3) might cause some restrictions for such measures in stands with small tree crowns. In terms of operationalization, currently reachable qualities to automatically retrieve tree crown segments from VHR data might also not yet suffice to make such texture measures a viable option. Concerning this, our classification maps might currently be sub-optimal as we trained the classifier with mean spectral values of

crown objects but predicted to pixels which are likely to be more heterogeneous as, for example, tree crowns often have a shaded and a sunlit part. This probably created some noise that could be reduced with a high-quality segmentation which we did not pursue in this study but would be the next step in further research.

Stand density

Stand density was successfully predicted by using two WorldView-2- derived variables including the number of local maxima and the fractions of coniferous, broadleaved, bare ground and shadow pixels. It can be assumed that in particular the local maxima approach is a comparably robust way to estimate stand density from VHR data; due to the very high spatial resolution of the WorldView-2 data, larger tree crowns become clearly visible in the image. The tree tops typically receive a higher amount of direct sunlight, which results in increased reflectance values and a detectable local maxima in contrast to the surrounding areas. However, this approach faces some limitations in the presence of overlapping or shaded tree crowns. A visual comparison of the derived local maxima with the visible tree crowns in the WorldView-2 data revealed that the rate of detection success was higher for larger and clearly identifiable crowns, while smaller and overlapping crowns were often missed. Accordingly, the approach appeared slightly more successful in coniferous than in broadleaved stands. Nevertheless, the number of derived maxima correlated well to the number of field measured trees. The local maxima approach has been suggested in various earlier studies, which also reported its general suitability to detect larger tree crowns (Gomes and Maillard, 2016; Patias and Stournara, 2016) and hence could additionally serve as a starting point for single tree delineations. In our case, the additional information on fractions of broadleaved, coniferous, shadow and bare ground pixels also contributed to the good model performance. In particular, the fractions of bare ground and shadow were found to be important predictors for tree density. The observed correlations matched well with the expectations, that is, higher stand density were observed for samples with lower fractions of bare ground and shadow.

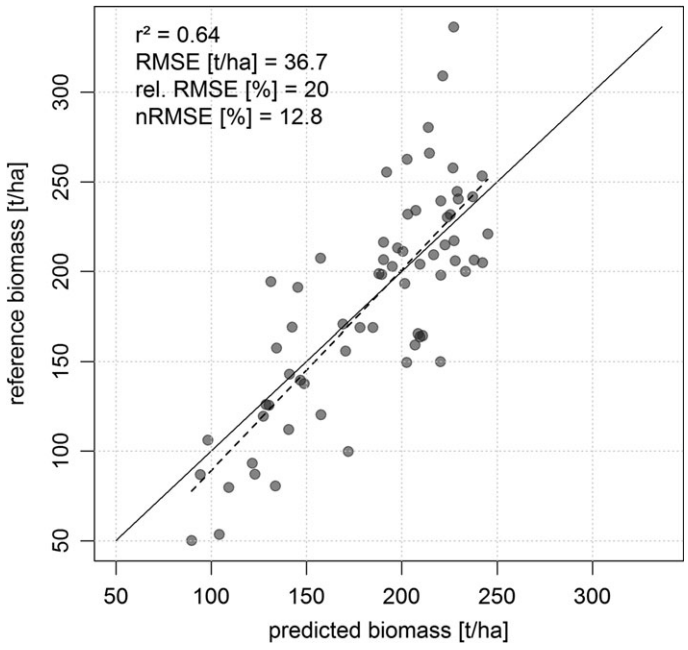

Figure 8 Scatterplot of predicted and observed biomass values. Solid line indicates the one-to-one line; dashed line indicates the linear model between values predicted by the Random Forest model and reference values.

An earlier LiDAR-based study in the same test site (Latifi *et al.*, 2012) reached relative RMSE rates of ~65 per cent when estimating stem density. This confirms that the potential of the WorldView-2 data to estimate tree density is good, although the reference datasets differed between the two studies and the LiDAR study was not optimized for tree detection but followed a rather general area-based approach.

Due to the simplicity of the presented approach and as also indicated by the very comparable results of the two WorldView-2 scenes, we expect the estimation of stand density to be quite robust. It might be possible to get reasonable spatial estimates of stand density even without calibrating the remote sensing data with explicit field data. Further research might head into this direction by for example just setting upper and lower limits of stand densities for a specific region (as often available from general forest inventories) and then creating a knowledge-based model based on the predictor variables of this study (fraction of bare ground, shadow, broadleaved and coniferous + the number of local maxima). Such a knowledge-based model could integrate

Table 7 Spearman rank correlation between predictor variables and biomass.

Predictor	Spearman rank correlation with field-estimated biomass – cloud-free scene	Spearman rank correlation with field-estimated biomass – clouded scene
Fraction of broadleaved trees	−0.45	−0.46
Fraction of coniferous trees	0.45	0.43
Fraction of shadow	0.46	0.48
Fraction of bare Ground	−0.13	−0.09
Local maxima (window size = 9)	−0.17	−0.14
Median height	0.37[1]	
Mean height	0.37[1]	
Standard deviation height	0.19[1]	

[1]Both scenes required to obtain the variable.

Table 8 Mean expert opinion score for LiDAR, hyperspectral (HS), very high resolution stereo-imagery (VHRSI) and stereo aerial photographs (Aerial Ph.) to operationally derive selected forest inventory variables.

	Species	Leaf chem.	Forest health	Single tree Del.	Height	Canopy cover	Multi-Layer det.	Stand density	Understorey	Wood volume	Mean (all var.)	Biome
LiDAR	1.7	1.0	1.4	**3.2**	**4.0**	**3.7**	**3.4**	**3.1**	**2.8**	**3.5**	**2.8**	All
HS	**3.0**	**3.0**	**3.1**	1.8	1.2	2.4	1.2	1.5	1.2	1.8	2.0	
VHRSI	2.5	1.7	2.4	2.4	2.7	3.0	1.2	2.2	1.3	2.6	2.2	
Aerial Ph.	2.4	1.4	2.4	2.9	3.0	3.2	1.5	2.5	1.4	2.6	2.3	
LiDAR	1.8	1.0	2.0	**3.4**	**4.0**	**4.0**	**3.4**	**3.4**	**2.6**	**3.8**	**2.9**	Boreal
HS	**2.8**	**2.5**	**3.0**	1.8	1.5	2.0	1.0	1.2	1.0	1.8	1.9	
VHRSI	2.4	1.2	2.5	2.6	2.8	2.8	1.0	2.0	1.0	2.8	2.1	
Aerial Ph.	**2.8**	1.2	2.8	3.0	3.4	3.0	1.6	2.4	1.0	3.0	2.4	
LiDAR	1.7	1.0	1.2	**3.1**	**3.9**	**3.7**	**3.2**	**2.8**	**2.8**	**3.4**	**2.7**	Temperate
HS	**3.1**	**2.9**	**3.1**	1.8	1.2	2.5	1.2	1.4	1.2	1.8	2.0	
VHRSI	2.5	1.8	2.3	2.3	2.9	2.9	1.1	2.2	1.2	2.8	2.2	
Aerial Ph.	2.4	1.4	2.3	2.8	3.1	3.2	1.3	2.4	1.4	2.5	2.3	
LiDAR	1.5	1.0	1.7	**3.2**	**4.0**	**3.2**	**3.8**	**3.5**	**2.8**	**3.8**	**2.8**	Tropical
HS	**3.2**	**3.5**	**3.7**	2.0	1.0	2.8	1.5	2.0	1.5	1.5	2.3	
VHRSI	2.5	2.0	2.7	2.2	1.8	3.2	1.8	2.5	2.0	2.0	2.3	
Aerial Ph.	2.0	1.3	2.0	3.0	2.2	3.5	2.0	3.0	1.8	2.2	2.3	

Bold numbers indicate highest scoring sensor type.

assumed relationships such as 'larger trees cast larger shadows, larger trees need more space, hence the density is lower' or 'young broadleaved stands build dense canopies and are less likely to show high fractions of bare ground, hence low fractions of bare ground indicate high stand densities in broadleaved forests'.

Biomass

With a RMSE of 36.7 t/ha the biomass estimates showed reasonable performance. Moreover, the performance was consistent with the results of an earlier LiDAR-based study across the study site (RMSE = 37.32 t/ha with a RF model in Latifi *et al.*, 2010), which shows the suitability of the applied VHRSI as a cost-effective surrogate to airborne LiDAR data for local area-based biomass estimates.

The selected predictor variables suggested that information on broadleaved/coniferous fractions were of highest relevance for biomass estimation, and were even more important than the information provided by the height. Species information has been frequently stated to be advantageous for biomass estimations due to the differences in species-dependent wood densities (see, e.g. Fassnacht *et al.*, 2014 and the reviewed references therein). However, in this study, the importance of species information can also be explained by the fact that many low biomass stands are comparably young, pure broadleaved stands, while highest biomass stands are often mixed stands with old-growth pine trees and an often two-layered structure. The latter point also explains the strong positive correlation of the fraction of shadow with field-estimated biomass values as especially these two-layered old growth pine stands showed notable fractions of shadow casted by the large pine trees. The importance of shadows for estimating biomass from VHR data has also been reported in earlier studies (Leboeuf *et al.*, 2007). One reason for the comparably low correlations of the height variables with biomass was the influence of a set of sample points with high height values but low biomass reference values (Supplementary Data 4). All of these samples were located in young and dense Red Oak stands. We hypothesize that within these stands two factors contributed to the observed patterns: (1) the VHRSI canopy height model might be less accurate in these stands as the applied photogrammetric matching relies on texture features that are detectable in both scenes; in very dense young broadleaved stands such features are sparse; (2) the high levels of competition in young and dense broadleaved stands often results in a small form factor of the individual trees and hence comparably high stand heights but low DBH and hence low biomass values. While most of these samples in young Red Oak stands could still be estimated with reasonable accuracies by integrating the predictor variables of broadleaved/coniferous fractions, the most extreme sample (very low field-estimated biomass value with high stand height) was excluded as one of the two outliers in the biomass model. The second outlier related to the problem of extrapolated field estimates being affected by large individual trees in otherwise young stands which has already been addressed in the methods section. Here, we tried to solve this problem by eliminating the 1 per cent trees with overall highest and lowest biomass values from the dataset. This step notably improved the correlation between the remote sensing signal and the field-based biomass estimates in our study. However, it is clearly not an optimal approach as also mirrored in the second outlier sample where the extrapolation problem still persisted after the outlier removal. Whenever possible, sample-based estimates should be avoided to train remote sensing models.

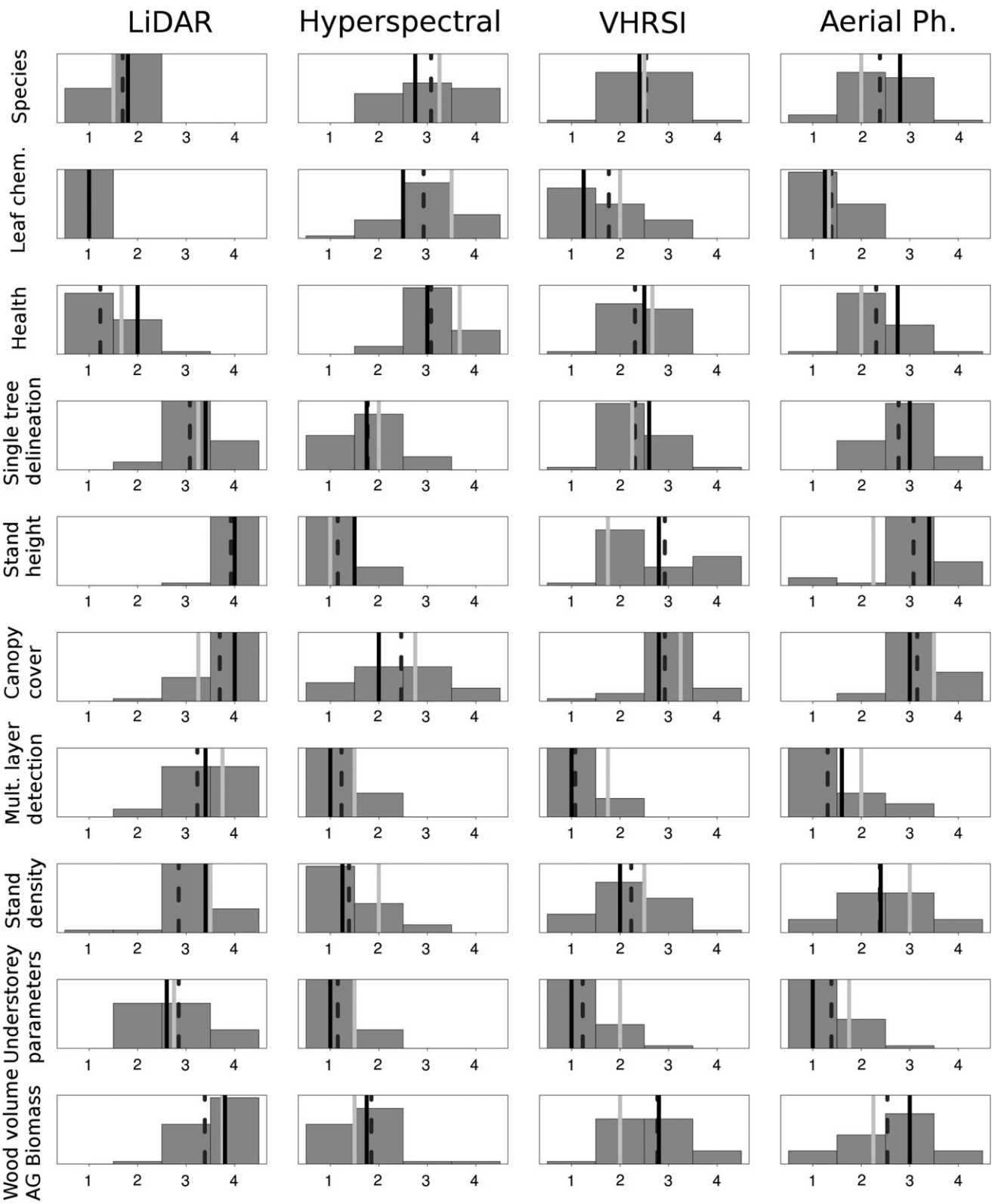

Figure 9 Summarized results of the expert opinion survey. The dashed black, grey and black stripes indicate mean values of temperate, boreal and tropical forests, respectively. Numbers below the histograms indicate the presumed potential with 1 = poor potential, 2 = limited potential, 3 = good potential and 4 = excellent potential.

Table 9 Shannon diversity of expert opinions on the suitability of LiDAR, hyperspectral (HS), very high resolution stereo-imagery (VHRSI) and stereo aerial photographs (Aerial Ph.) to operationally derive selected forest inventory variables.

	Species	Leaf chem.	Forest health	Single tree del.	Height	Canopy cover	Multi-Layer det.	Stand density	Understorey	Wood volume	Mean (all var.)
LiDAR	0.63	0.00	0.82	0.86	0.18	0.71	**0.93**	0.88	1.04	0.82	0.69
HS	**1.09**	**1.14**	0.86	**0.98**	0.49	**1.33**	0.55	0.88	0.49	1.00	0.88
VHRSI	1.00	1.04	0.86	0.96	**1.15**	0.86	0.47	1.17	0.71	1.14	0.94
Aerial Ph.	1.08	0.65	**0.97**	0.94	0.98	0.86	0.90	**1.28**	**0.76**	**1.26**	**0.97**

Bold numbers indicate highest Shannon diversity value for a given forest inventory variable.

One major constraint of the presented study are the explicit characteristics of the test site which limit its representativeness for temperate European forest stands. One of these characteristics is topography: whereas the Central European mixed stands are mostly characterized by mountainous or hilly terrain, the study site is associated with a very low topographic gradient in which the geometric terrain effects on the quality of passive spectral imagery can be considered as minimal. A further phenomenal issue concerns the forest types: the study site comprises an untypically high number of tree species in mixture compared with common forest stands in the region. Besides the stands with only a single tree species (Pine, Beech or Oak), various mixtures occur in the site, ranging from separate groups of broadleaves or coniferous trees to mixed stands of both species groups. This highlights one of the crucial advantages of the applied methodology, namely the potential of the applied WorldView-2 imagery for detailed tree type mapping. Coupled with the subsequent biomass models, it forms a practically efficient processing chain in which species-specific biomass can be retrieved by the use of only one remotely sensed data source. This is a complement to the existing area-based LiDAR methods (Latifi *et al.*, 2015), which generally lack a built-in species classification, and should therefore only rely on either sample-based forest inventory data or species information provided by additional spectral data.

In addition, one may note that an approach solely based on VHRSI for retrieving structural attributes is dependent on an already existing LiDAR-based DTM to normalize the heights and produce a nDSM, which in turn constrains a practical application. Finally, the results in this study were produced with a repeat-pass stereo imagery, in which a longer time lag exists between the acquired panchromatic and multispectral images compared with single-pass data. Due to reduced decorrelation issues when using single pass data, the results might be improved if single pass imagery would be used.

Expert opinions on practical application

To give insight in the current opinions of the remote sensing community about the potential for practical application of airborne LiDAR, hyperspectral and multispectral data as well as VHRSI data to automatically retrieve forest variables we conducted a brief expert opinion survey. We received notably more opinions (13 replies) on temperate forests than for boreal and tropical forests (4 and 5 replies, respectively). This result is a consequence of the often strong focus of the VHR and airborne remote sensing community on temperate forest ecosystems which relates to the location of many research groups in this field.

The results of the survey showed that especially for LiDAR data, the expert opinions agreed well amongst each other as indicated by a low mean Shannon Index (SI) value (0.69). Highest diversity values and hence most strongly varying opinions were observed for 'Multi-Layer Detection' and 'Understorey Detection'. These parameters have been investigated in earlier studies (Hill and Broughton, 2009; Latifi *et al.*, 2017) but as they are mostly relevant for ecological questions they are still less well investigated than economically relevant forest inventory attributes such as growing stock or biomass. The homogeneous tendencies observed in the opinions on the potential of LiDAR data might be related to the nature of the sensor system (very well suited for structure and hardly suited for optical traits) but partly also to the huge amount of literature that has been published on LiDAR applications in forests.

Concerning the potential of LiDAR, experts judged that LiDAR data has only poor or limited potential (mean scores between 1.0 and 1.7) to obtain parameters that are predominantly related to spectral information including 'Leaf chemicals', 'Forest health', and 'Species'. On the other hand, all variables predominantly related to structure received high scoring rates (2.8–4.0).

The opinions on the potential of hyperspectral data were more diverse as indicated by a mean SI of 0.88. Opinions were especially diverse for 'Canopy Cover' (SI = 1.33), 'Leaf Chemistry' (SI = 1.14) and 'Species' (SI = 1.09). It is interesting to see that the experts' opinion on the potential of hyperspectral data are quite diverse even concerning its assumed prime disciplines 'Species' and 'Leaf Chemistry' which both also received several votes for the 'limited' category. However, at least for 'Leaf Chemistry' this also reflects an ongoing discussion in the remote sensing community about the direct estimation of for example nitrogen from hyperspectral data, which has been the subject to much debate (Knyazikhin *et al.*, 2013). Another reason for this rather critical view was revealed in the comments of one of the returned forms which pointed out that limited data availability is hampering any operational use of hyperspectral data. Furthermore, the application of hyperspectral data to retrieve some of the listed variables such as 'Canopy Cover', 'Understory Detection' or 'Stand Density' has also been rarely investigated.

Opinions on the potential of VHRSI are even more diverse than for the hyperspectral data (mean SI = 0.94). Most diverse scores were observed for 'Stand Density' (SI = 1.17), 'Stand Height' (SI = 1.15) and 'Wood Volume/Biomass' (SI = 1.14). In our opinion, this reflects the current state of knowledge quite well. The number of studies applying VHRSI data is still comparably low and hence the experts are less familiar with these data.

Therefore, clear opinions on the real potential of these data have not yet been formed in the remote sensing community. Nevertheless, it is interesting to see that only three forest attributes including 'Multi-layer Detection', 'Understory Detection' and 'Leaf Chemistry' received mean scores of less than two. All other forest attributes received at least one vote for 'good' (score of 3) or 'excellent' (score of 4) potential. This indicates that further research in this area is required.

For aerial images, we observed similarly diverse opinions as for the VHRSI with an even slightly higher mean SI of 0.97. Most diverse opinions were observed for 'Stand Density', 'Wood Volume/Biomass' and 'Leaf Chemistry'. Highest potential was assumed for the estimation of 'Canopy Cover' (mean score = 3.2) and 'Stand Height' (mean score = 3.0). Here, similarly as for VHRSI, the full potential of most recent datasets and processing approaches might have not yet been described as the number of recent studies focusing on this data type is limited. One reason for this might be that, the application of aerial images has a somewhat 'old-fashioned' touch in the remote sensing community. Nevertheless, very recent studies have pointed out how valuable these – in many cases already existing data – can be if analyzed with newly available photogrammetric and image processing algorithms (Rahlf *et al.*, 2014; Stepper *et al.*, 2015a,b; Straub and Stepper, 2016).

VHRSI data for practitioners

As expected, none of our individual results for modelling stand density and biomass or for classifying tree species showed a strong improvement over earlier results obtained with LiDAR (Latifi *et al.*, 2012, 2015; Fassnacht *et al.*, 2014) or hyperspectral data (Ghosh *et al.*, 2014; Fassnacht *et al.*, 2014) in the same study area. However, we think that from a practitioner's perspective, VHRSI data offer some important advantages over these airborne datasets:

First of all, the acquisition of VHRSI is relatively fast and easy to accomplish. After placing an online order, there might be a certain time delay due to weather conditions and competing acquisitions in the same orbit. However, once the data are acquired, it is typically delivered within a few days after the image acquisition. A notable advantage of VHRSI data over airborne data is the global availability of on-demand data, while companies offering airborne LiDAR and hyperspectral acquisitions are still rare in many parts of the world.

For a local to regional application with a single pair of VHR scenes, no further pre-processing of the VHRSI is required if a geometrically orthorectified product has been ordered. Several earlier studies showed that atmospheric correction procedures are not necessary for most applications (excluding change-detection or physical-based approaches) if a single optical dataset is used in combination with field data (Pu *et al.*, 2015). This is a consequence of the acquisition from space that takes place during a single satellite overflight and within a small time-span during which atmospheric conditions typically remain stable resulting in a homogeneous atmospheric effect on the obtained image. In comparison, to cover the area of a typical VHRSI acquisition (starting at 100 km²) with an airborne hyperspectral campaign, many overlapping flight lines have to be acquired, co-registered and pre-processed. In many cases, the pre-processing is not fully automated and the correction for varying observation geometries, weather conditions, etc. is time-consuming and requires sophisticated professional software. Hence practitioners might face the problem to either work with the delivered data quality from the data provider or being obliged to learn complex pre-processing steps of hyperspectral data which is not likely to happen. Obviously, the previously discussed stability of atmospheric conditions during a VHRSI acquisition does not solve problems related to terrain shadows that can severely hamper automated analysis of VHRSI data or at least force a prior stratification into shaded and non-shaded parts for all analytical steps.

A further advantage of VHRSI data is that they are comparably more convenient to handle and understand. Most practitioners are familiar with airborne multispectral data (orthophotos and digital aerial imagery) which are typically delivered in the same data formats as VHRSI data. An intuitive integration of the VHRSI data into existing GIS systems should therefore be possible and hence, besides serving as a data source for automated analysis, VHRSI data can also be used for traditional photo-interpretation purposes (albeit the spatial resolution with a current maximum of 0.3 m might be slightly coarser than recent airborne datasets). On the contrary, the high dimensionality of hyperspectral data and the 3D-nature of LiDAR data might pose problems to practitioners with less experience in handling these kinds of data formats.

Despite the listed advantages, VHRSI cannot match airborne data in certain aspects. Particularly, LiDAR data offers some functional characteristics such as the possibility to extract a DTM and delivering insights into the structure of stands and thereby enabling to assess multi-layered stands and understory parameters. In the present study, we applied a LiDAR DTM in combination with the DSM calculated from the VHRSI to derive vegetation heights. In flat terrain it might be possible to make use of canopy gaps to calculate a DTM from a photogrammetric point cloud. However, the quality of a DTM derived by LiDAR data can obviously not be reached with such approaches. On the other hand, if a LiDAR DTM is available, retrieving an accurate estimate of stand height can be accomplished with VHRSI and this might already match most important information demands of practitioners.

Depending on the required level of detail, the spectral information contained in the VHR data might also be too low to adequately characterize the species composition of forest stands. While the applied WorldView-2 dataset with eight spectral bands covering the visual and a part of the near-infrared domains showed good potential to separate several dominating tree species in the study area, other VHR satellite systems that often deliver spectral information in only four bands are likely to not surpass a discrimination of forest stands into broad categories such as broadleaved, coniferous and mixed or in best case a discrimination of few dominating tree species as demonstrated in Immitzer *et al.* (2012). Whether this is a real drawback for practitioners can be questioned. For many applications an accurate stand-wise estimation of broadleaved to coniferous ratio might already be valuable.

Conclusion

In this study, we tested the application of VHRSI obtained by WorldView-2 to estimate forest stand density and biomass as

well as to classify tree species over a temperate mixed forest in Germany. For the estimation of stand density and biomass, the presented approach utilizing the RF algorithm with three groups of predictor variables, including height information obtained from a photogrammetric point cloud, fractions of broadleaved, coniferous, shadow and bare ground pixels (resulting from a supervised classification) and the number of local maxima (obtained from the panchromatic band of the WorldView-2 data) delivered good results over the examined test site that had flat topography.

The results of tree species classification considering five dominant tree species did not achieve accuracies that were formerly achieved by applying hyperspectral data over the same test site. However, the achieved accuracies of over 80 per cent were still reasonable, and the obtained species maps agreed well with the field observations within pure stands. Furthermore, the discrimination of broadleaved and coniferous trees was possible with nearly perfect accuracies, underlining the potential of spaceborne VHR data for continuous mapping of forest types.

Finally, the results of the expert opinion survey suggested that while opinions on the operational potential of LiDAR and hyperspectral data are already quite firmly formed, the potential of VHR optical stereo data is probably still not fully understood, as indicated by contrasting opinions on the potential of these data to estimate important forest attributes such as stand height that received almost equal number of votes for excellent and poor potential.

By considering our experimental and survey results, we call for further research on the application of spaceborne and airborne VHR stereo-images to obtain forest inventory parameters using automated approaches.

Supplementary data

Supplementary data are available at *Forestry* online.

Acknowledgements

We would like to acknowledge the following colleagues who participated in the expert opinion survey: Gregory Asner, Clement Atzberger, Johannes Breidenbach, Fabio Marcelo Breunig, Matthew Clark, Nicholas Coops, Michele Dalponte, Laura Duncanson, Michael Falkowski, Terje Gobakken, Andrew T. Hudak, Michael Keller, Ilkka Korpela, Joachim Maack, Erik Næsset, Hans Ole Ørka, Henrik Persson, Arijit Roy, Christoph Straub, Lars Waser. Furthermore, we are grateful to an anonymous reviewer and to Gary Kerr, who gave valuable comments to improve earlier versions of this article.

Conflict of interest statement

None declared.

Funding

German National Space Agency DLR (Deutsches Zentrum für Luft- und Raumfahrt e.V.) on behalf of the German Federal Ministry of Economy and Technology on the basis of a decision by the German Bundestag. Support code: 50EE1265.

References

Alonzo, M., Bookhagen, B. and Roberts, D.A. 2014 Urban tree species mapping using hyperspectral and lidar data fusion. *Remote Sens. Environ.* **148**, 70–83.

Annighöfer, P., Mölder, I., Zerbe, S., Kawaletz, H., Terwei, A. and Ammer, C. 2012 Biomass functions for the two alien tree species *Prunus serotina* Ehrh. and *Robinia pseudoacacia* L. in floodplain forests of Northern Italy. *Eur. J Forest Res.* **131** (5), 1619–1635.

Beasom, S.L. and Haucke, H.H. 1975 A comparison of four distance sampling techniques in South Texas live oak mottes. *J. Range Manage.* **28** (2), 142–144.

Beguet, B., Guyon, D., Boukir, S. and Chehata, N. 2014 Automated retrieval of forest structure variables based on multi-scale texture analysis of VHR satellite imagery. *ISPRS J. Photogramm. Remote Sens.* **96**, 164–178.

Breiman, L. 2001 Random forests. *Mach. Learn.* **45**, 5–32.

Chirici, G., Giuliarelli, D., Biscontini, D., Tonti, D., Mattioli, W., Marchetti, M., *et al*. 2011 Large-scale monitoring of coppice forest clearcuts by multitemporal very high resolution satellite imagery. A case study from central Italy. *Remote Sens. Environ.* **115**, 1025–1033.

Cho, M.A., Malahlela, O. and Ramoelo, A. 2015 Assessing the utility WorldView-2 imagery for tree species mapping in South African subtropical humid forest and the conservation implications: Dukuduku forest patch as case study. *Int. J. Appl. Earth Obs. Geoinf.* **38**, 349–357.

Clark, M.L., Clark, D.B. and Roberts, D.A. 2004 Small-footprint lidar estimation of sub-canopy elevation and tree height in a tropical rain forest landscape. *Remote Sens. Environ.* **91** (1), 68–89.

Clark, M.L., Roberts, D.A. and Clark, D.B. 2005 Hyperspectral discrimination of tropical rain forest tree species at leaf to crown scales. *Remote Sens. Environ.* **96** (3–4), 375–398.

Clevers, J.G., Kooistra, L. and Schaepman, M.E. 2010 Estimating canopy water content using hyperspectral remote sensing data. *Int. J. Appl. Earth Obs. Geoinf.* **12** (2), 119–125.

Coops, N., Stanford, M., Old, K., Dudzinski, M., Culvenor, D. and Stone, C. 2003 Assessment of dothistroma needle blight of Pinus radiata using airborne hyperspectral imagery. *Phytopathology.* **93** (12), 1524–1532.

Dalponte, M., Ørka, H.O., Ene, L.T., Gobakken, T. and Næsset, E. 2014 Tree crown delineation and tree species classification in boreal forests using hyperspectral and ALS data. *Remote Sens. Environ.* **140**, 306–317.

Dalponte, M., Reyes, F., Kandare, K. and Gianelle, D. 2015 Delineation of individual tree crowns from ALS and hyperspectral data: a comparison among four methods. *Eur. J. Remote Sens.* **28**, 365–382.

Dian, Y., Pang, Y., Dong, Y. and Li, Z. 2016 Urban tree species mapping using airborne LiDAR and hyperspectral data. *J. Indian Soc. Remote Sens.* **44** (4), 595–603.

Dubayah, R.O., Sheldon, S.L., Clark, D.B., Hofton, M.A., Blair, J.B., Hurtt, G. C., *et al*. 2010 Estimation of tropical forest height and biomass dynamics using lidar remote sensing at La Selva, Costa Rica. *J. Geophys. Res.* **115** (G2), G00E09.

Hastie, T., Tibshirani, R. and Friedman, J. 2009 *The Elements of Statistical Learning: Data Mining, Inference, and Prediction*. 2nd edn.. Springer.

Hill, R.A. and Broughton, R.K. 2009 Mapping the understorey of deciduous woodland from leaf-on and leaf-off airborne LiDAR data: a case study in lowland Britain. *ISPRS J. Photogram. Remote Sens.* **64**, 223–233.

Holopainen, M., Vastaranta, M. and Hyyppä, J. 2014 Outlook for the next generation's precision forestry in Finland. *Forests* **5**, 1682–1694.

Fassnacht, F.E., Neumann, C., Foerster, M., Buddenbaum, H., Ghosh, A., Clasen, A., *et al*. 2014 Comparison of feature reduction algorithms for

classifying tree species with hyperspectral data on three Central European test sites. *IEEE J. Sel. Top. Appl. Earth Obs. Remote Sens.* **7** (6), 2547–2561.

Fassnacht, F.E., Li, L. and Fritz, A. 2015 Mapping degraded grassland on the Eastern Tibetan Plateau with multi-temporal Landsat 8 data - where do the severely degraded areas occur? *Int. J. Appl. Earth Obs. Geoinf.* **42**, 115–127.

Fassnacht, F.E., Latifi, H., Sterenczak, K., Modzelewska, A., Lefsky, M., Waser, L.T., *et al*. 2016 Review of studies on tree species classification from remotely sensed data. *Remote Sens. Environ.* **186**, 64–87.

Falkowski, M.J., Smith, A.M.S., Hudak, A.T., Gessler, P.E., Vierling, L.A. and Crookston, N.L. 2006 Automated estimation of indvidual conifer tree height and crown diameter via two-dimensional spatial eavelet analysis of lida data. *Can. J. Remote Sens.* **32** (2), 153–161.

Ghosh, A., Fassnacht, F.E., Joshi, P.K. and Koch, B. 2014 A framework for mapping tree species combining hyperspectral and LiDAR data: Role of selected classifiers and sensor across three spatial scales. *Int. J. Appl. Earth Obs. Geoinf.* **26**, 49–63.

Gomes, M.F. and Maillard, P. 2016 Detection of tree crowns in very high spatial resolution images. In *Environmental Applications of Remote Sensing*. M. Marghany (ed). INTECH, pp. 41–71. Chapter 2.

Heinzel, J. and Koch, B. 2011 Exploring full-waveform LiDAR parameters for tree species classification. *Int. J. Appl. Earth Obs. Geoinf.* **13** (1), 152–160.

Hudak, A.T., Strand, E.K., Vierling, L.A., Byrne, J.C., Eitel, J.U.H., Martinuzzi, S., *et al*. 2012 Quantifying aboveground forest carbon pools and fluxes from repeat LiDAR surveys. *Remote Sens. Environ.* **123**, 25–40.

Immitzer, M., Stepper, C., Böck, S., Straub, C. and Atzberger, C. 2016 Use of WorldView-2 stereo imagery and National Forest Inventory data for wall-to-wall mapping of growing stock. *Forest Ecol. Manage.* **359**, 232–246.

Immitzer, M. and Atzberger, C. 2014 Early detection of bark beetle infestation in Norway Spruce (Picea abies, L.) using WorldView-2 data. *Photogramm. Fernerkun.Geoinf.* **5**, 351–367.

Immitzer, M., Atzberger, C. and Koukal, T. 2012 Tree species classification with random forest using very high spatial resolution 8-band WorldView-2 satellite data. *Remote Sens.* **4** (9), 2661–2693.

ITT Visual Information Solutions, 2009 ENVI 4.7 SP2.

Jenkins, J.C., Chojnacky, D.C., Heath, L.S. and Birdsey, R.A. 2003 National-scale biomass estimators for United States tree species. *Forest Sci.* **49** (1), 12–35.

Kalacska, M., Lalonde, M. and Moore, T.R. 2015 Estimation of foliar chlorophyll and nitrogen content in an ombrotrophic bog from hyperspectral data: scaling from leaf to image. *Remote Sens. Environ.* **169**, 270–279.

Kattenborn, T., Maack, J., Fassnacht, F.E., Enßle, F., Ermert, J. and Koch, B. 2015 Mapping forest biomass from space—fusion of hyperspectral EO1-hyperion data and Tandem-X and WorldView-2 canopy height models. *Int. J. Appl. Earth Obs. Geoinf.* **35**, 359–367.

Knyazikhin, Y., Schull, M.A., Stenberg, P., Mõttus, M., Rautiainen, M., Yang, Y., *et al*. 2013 Hyperspectral remote sensing of foliar nitrogen content. *Proc. Natl. Acad. Sci.* **110** (3), E185–E192.

Korpela, I., Ørka, H.O., Maltamo, M., Tokola, T. and Hyyppä, J. 2010 Tree species classification using airborne LiDAR—effects of stand and tree parameters, downsizing of training set, intensity normalization, and sensor type. *Silva Fenn.* **44** (2), 319–339.

Lagomasino, D., Fatoyinbo, T., Lee, S.K., Feliciano, E., Trettin, C. and Simard, M. 2016 A comparison of mangrove canopy height using multiple independent measurements from land, air, and space. *Remote Sens.* **8**, 327.

Latifi, H., Hill, S., Schumann, B., Heurich, M. and Dech, S. 2017 Multi-model estimation of understorey shrub, herb and moss cover in temperate forest stands by laser scanner data. *Forestry*. doi:10.1093/forestry/cpw066.

Latifi, H., Fassnacht, F.E., Hartig, F., Berger, C., Hernández, J., Corvalán, P., *et al*. 2015 Stratified aboveground forest biomass estimation by remote sensing data. *Int. J. Appl. Earth Obs. Geoinf.* **38**, 229–241.

Latifi, H., Fassnacht, F.E. and Koch, B. 2012 Forest structure modeling with combined airborne hyperspectral and LiDAR data. *Remote Sens. Environ.* **121**, 10–25.

Latifi, H., Nothdurft, A. and Koch, B. 2010 Non-parametric prediction and mapping of standing timber volume and biomass in a temperate forest: application of multiple optical/LiDAR-derived predictors. *Forestry* **83**, 395–407.

Leboeuf, A., Beaudoin, A., Fournier, R.A., Guindon, L., Luther, J.E. and Lambert, M.-C. 2007 A shadow fraction method for mapping biomass of northern boreal black spruce forests using QuickBird imagery. *Remote Sens. Environ.* **110**, 488–500.

Lim, K., Treitz, P., Wulder, M., St-Onge, B. and Flood, M. 2003 LiDAR remote sensing of forest structure. *Prog. Phys. Geogr.* **27** (1), 88–106.

Lopatin, J., Dolos, K., Hernández, J., Galleguillos, M. and Fassnacht, F.E. 2016 Comparing generalized linear models and random forest to model vascular plant species richness using LiDAR data in a natural forest in central Chile. *Remote Sens. Environ.* **173**, 200–210.

Lucas, K.L., Raber, G.T. and Carter, G.A. 2010 Estimating vascular plant species richness on Horn Island, Mississippi using small-footprint airborne LIDAR. *J. Appl. Remote Sens.* **4** (1), 043545.

Maack, J., Kattenborn, T., Ewald Fassnacht, F., Enssle, F., Hernández Palma, J., Corvalán Vera, P., *et al*. 2015 Modeling forest biomass using very-high-resolution data-combining textural, spectral and photogrammetric predictors derived from spaceborne stereo images. *Eur. J. Remote Sens.* **48**, 245–261.

Man, Q., Dong, P., Guo, H., Liu, G. and Shi, R. 2014 Light detection and ranging and hyperspectral data for estimation of forest biomass: a review. *J. Appl. Remote Sens.* **8** (1), 081598.

McRoberts, R.E., Næsset, E. and Gobakken, T. 2013 Inference for lidar-assisted estimation of forest growing stock volume. *Remote Sens. Environ.* **128**, 268–275.

Mitchell, K. 2001 (revised 2015) *Quantitative Analysis by the Point-Centered Quarter Method*. Hobart and William Smith Colleges, Geneva, NY, US. https://arxiv.org/pdf/1010.3303.pdf (accessed on 10 December, 2016)

Næsset, E., Gobakken, T., Bollandsåsa, O.M., Gregoire, T.G., Nelson, R. and Ståhl, G. 2013 Comparison of precision of biomass estimates in regional field sample surveys and airborne LiDAR-assisted surveys in Hedmark County, Norway. *Remote Sens. Environ.* **130**, 108–120.

Nilsson, M. 1996 Estimation of tree heights and stand volume using an airborne lidar system. *Remote Sens. Environ.* **56** (1), 1–7.

Ørka, H.O., Næsset, E. and Bollandsås, M. 2009 Classifying species of individual trees by intensity and structure features derived from airborne laser scanner data. *Remote Sens. Environ.* **113** (6), 1163–1174.

Ørka, H.O. and Hauglin, M. 2016 Use of remote sensing for mapping of non-native conifer species. *INA Fagrapport 33*, 76 pp.

Ozdemir, I. and Karnieli, A. 2011 Predicting forest structural parameters using the image texture derived from WorldView-2 multispectral imagery in a dryland forest, Israel. *Int. J. Appl. Earth Obs. Geoinf.* **13**, 701–710.

Patias, P. and Stournara, P. 2016 Estimating wood volume for Pinus brutia trees in forest stands from Quickbird-2 imagery. *The International Archives of the Photogrammetry, Remote Sensing and Spatial Information Sciences*, Volume XLI-B7, 2016 XXIII ISPRS Congress, 12–19 July 2016, Prague, Czech Republic.

Peerbhay, K.Y., Mutanga, O. and Ismail, R. 2014 Investigating the capability of few strategically placed worldview-2 multispectral bands to discriminate Forest species in KwaZulu-Natal, South Africa. *IEEE J. Sel. Top. Appl. Earth Obs. Remote Sens.* **7** (1), 307–316.

Persson, H.J. and Perko, R. 2016 Assessment of boreal forest height from WorldView-2 satellite stereo images. *Remote Sens. Lett.* **7** (12), 1150–1159.

Persson, H.J. 2016 Estimation of boreal forest attributes from very high resolution Pléiades data. *Remote Sens.* **8**, 736.

Pontius, J., Martin, M., Plourde, L. and Hallett, R. 2008 Ash decline assessment in emerald ash borer-infested regions: a test of tree-level hyperspectral technologies. *Remote Sens. Environ.* **112**, 2665–2676.

Pu, R. and Cheng, J. 2015 Mapping forest leaf area index using reflectance and textural information derived from WorldView-2 imagery in a mixed natural forest area in Florida, US. *Int. J. Appl. Earth Obs. Geoinf.* **42**, 11–23.

Pu, R. and Landry, S. 2012 A comparative analysis of high spatial resolution IKONOS and WorldView-2 imagery for mapping urban tree species. *Remote Sens. Environ.* **124**, 516–533.

Pu, R., Landry, S. and Zhang, J. 2015 Evaluation of atmospheric correction methods in identifying urban tree species with WorldView-2 imagery. *IEEE J. Sel. Top. Appl. Earth Obs. Remote Sens.* **8** (5), 1886–1897.

Rahlf, J., Breidenbach, J., Solberg, S., Næsset, E. and Astrup, R. 2014 Comparison of four types of 3D data for timber volume estimation. *Remote Sens. Environ.* **155**, 325–333.

Schlerf, M., Atzberger, C., Hill, J., Buddenbaum, H., Werner, W. and Schüler, G. 2010 Retrieval of chlorophyll and nitrogen in Norway spruce (Picea abies L. Karst.) using imaging spectroscopy. *Int. J. Appl. Earth Obs. Geoinf.* **12** (1), 17–26.

Stepper, C., Straub, C. and Pretzsch, H. 2015a Using semi-global matching point clouds to estimate growing stock at the plot and stand levels: application for a broadleaf-dominated forest in central Europe. *Can. J. Forest Res.* **45** (1), 111–123.

Stepper, C., Straub, C., Immitzer, M. and Pretzsch, H. 2016 Using canopy heights from digital aerial photogrammetry to enable spatial transfer of forest attribute models: a case study in central Europe. *Scand. J. Forest Res.* **0**, 1–48.

Stepper, C., Straub, C. and Pretzsch, H. 2015b Assessing height changes in a highly structured forest using regularly acquired aerial image data. *Forestry* **88**, 304–316.

Straub, C. and Koch, B. 2011 Estimating single tree stem volume of pinus sylvestris using airborne laser scanner and multispectral line scanner data. *Remote Sens.* **3** (5), 929–944.

Straub, C., Tian, J., Seitz, R. and Reinartz, P. 2013 Assessment of Cartosat-1 and WorldView-2 stereo imagery in combination with a LiDAR-DTM for timber volume estimation in a highly structured forest in Germany. *Forestry* **86** (4), 463–473.

Straub, C. and Stepper, C. 2016 Using digital aerial photogrammetry and the random forest approach to model forest inventory attributes in Beech- and Spruce-dominated Central European Forests. *Photogramm. Fernerkund. Geoinf.* **3**, 109–123.

Tomaštík, J. Jr, Tomaštík, J. Sr, Saloň, Š. and Piroh, R. 2016 Horizontal accuracy and applicability of smartphone GNSS positioning in forests. *Forestry*. doi:10.1093/forestry/cpw031.

Vaughn, N.R., Moskal, L.M. and Turnblom, E.C. 2012 Tree species detection accuracies using discrete point lidar and airborne waveform lidar. *Remote Sens.* **4** (2), 377–403.

Waser, L.T., Klonus, S., Ehlers, M., Küchler, M. and Jung, A. 2010 Potential of digital sensors for land cover and tree species classifications—a case study in the framework of the DGPF-project. *Photogramm. Fernerkund. Geoinf.* **2010** (2), 141–156.

Waser, L.T., Küchler, M., Jütte, K. and Stampfer, T. 2014 Evaluating the potential of WorldView-2 data to classify tree species and different levels of ash mortality. *Remote Sens.* **6** (5), 4515–4545.

Weinacker, H., Koch, B. and Weinacker, R. 2004 TREESVIS—a software system for simultaneous 3D-realtime visualization of DTM, DSM, laser raw data, multispectral data, simple tree and building models. *Int. Arch. Photogram. Remote Sens. Spatial Inf. Sci.* **36**, 90–95. Freiburg, Germany (Part 8/W2).

Zell, J. 2008 *Methoden für die Ermittlung, Modellierung und Prognose der Kohlenstoffspeicherung in Wäldern auf Grundlage permanenter Großrauminventuren*. Ph.D dissertation, Faculty of Forest and Environmental Studies, University of Freiburg, 162 pp. (in German with English summary).

Zhang, K. and Hu, B. 2012 Individual urban tree species classification using very high spatial resolution airborne multi-spectral imagery using longitudinal profiles. *Remote Sens.* **4**, 1741–1757.

Zhang, C. and Qiu, F. 2012 Mapping individual tree species in an urban forest using airborne Lidar data and hyperspectral imagery. *Photogramm. Eng. Remote Sens.* **78** (10), 1079–1087.

Zianis, D., Muukkonen, P., Mäkipää, R. and Mencuccini, M. 2005 *Silva Fennica Monographs*. Bd. 4, 2005*:* Biomass and Stem Volume Equations for Tree Species in Europe. Finnish Society of Forest Science, Finnish Forest Research Institute.

Zhou, J.-J., Zhao, Z., Zhao, J., Zhao, Q., Wang, F. and Wang, H. 2014 A comparison of three methods for estimating the LAI of black locust (*Robinia pseudoacacia* L.) plantations on the Loess Plateau, China. *Int. J. Remote Sens.* **35**, 171–188.